Generalizations of the Kerr-Newman solution

Contents

1 Topics

- Generalizations of the Kerr-Newman solution

1.1 ICRANet Participants

- Donato Bini
- Andrea Geralico
- Roy Kerr
- Remo Ruffini

1.2 Ongoing collaborations

- Hernando Quevedo (Universidad Nacional Autónoma de México, Mexico)

1.3 Students

- Kuantay Boshkayev (IRAP PhD, Kazakhstan)
- Wenbiao Han (IRAP PhD, China)
- Orlando Luongo (Rome University PhD, Italy)
- Daniela Pugliese (Rome University PhD, Italy)

2 Brief description

One of the most important metrics in general relativity is the Kerr-Newman solution which describes the gravitational and electromagnetic fields of a rotating charged mass. For astrophysical purposes, however, it is necessary to take into account the effects due to the moment of inertia of the object. To attack this problem we have derived exact solutions of Einstein-Maxwell equations which posses an infinite set of gravitational and electromagnetic multipole moments.

To study the physical relevance of such solutions in the context of relativistic astrophysics we analyze the particular case of a rotating mass with an arbitrary quadrupole moment. The investigation of the motion of test particles in the corresponding gravitational field shows that the quadrupole drastically affects the structure of spacetime. In particular, effects associated with repulsive gravity take place due to the presence of naked singularities. We perform an analytical study of circular motion around naked singularities in the specific case of the Reissner-Nordström spacetime. To study the physical effects of repulsive gravity in an invariant manner we propose to use the eigenvalues of the curvature tensor which are scalar quantities and provide physically reasonable results in the case of naked singularities with black hole counterparts as well as in the case of naked singularities generated by higher multipole moments.

We study the problem of the interior solution for a rotating mass with quadrupole moment. In particular, we show that the approximate interior Hartle-Thorne solution can be matched with an approximate exterior solution which is a particular case of the exact Mashhoon–Quevedo exterior solution. The quadrupole parameter is interpreted as an additional degree of freedom that can be used to attack the problem of finding physically reasonable interior solutions. We study the Zipoy-Voorhees static solution and find a particular interior counterpart which is described by a static perfect fluid with quadrupole moment. We also study the problem of matching stationary and axisymmetric exterior and interior solutions, and propose an invariant approach based upon the use of curvature invariants.

3 Introduction

It is hard to overemphasize the importance of the Kerr geometry not only for general relativity itself, but also for the very fundamentals of physics. It assumes this position as being the most physically relevant rotating generalization of the static Schwarzschild geometry. Its charged counterpart, the Kerr-Newman solution, representing the exterior gravitational and electromagnetic fields of a charged rotating object, is an exact solution of the Einstein-Maxwell equations.

Its line element in Boyer–Lindquist coordinates can be written as

$$\begin{aligned} ds^2 &= \frac{r^2-2Mr+a^2+Q^2}{r^2+a^2\cos^2\theta}(dt-a\sin^2\theta d\varphi)^2 \\ &\quad -\frac{\sin^2\theta}{r^2+a^2\cos^2\theta}[(r^2+a^2)d\varphi-adt]^2 \\ &\quad -\frac{r^2+a^2\cos^2\theta}{r^2-2Mr+a^2+Q^2}dr^2-(r^2+a^2\cos^2\theta)d\theta^2\,, \end{aligned} \tag{3.0.1}$$

where M is the total mass of the object, $a = J/M$ is the specific angular momentum, and Q is the electric charge. In this particular coordinate system, the metric functions do not depend on the coordinates t and ϕ, indicating the existence of two Killing vector fields $\xi^I = \partial_t$ and $\xi^{II} = \partial_\varphi$ which represent the properties of stationarity and axial symmetry, respectively.

An important characteristic of this solution is that the source of gravity is surrounded by two horizons situated at a distance

$$r_\pm = M \pm \sqrt{M^2-a^2-Q^2} \tag{3.0.2}$$

from the origin of coordinates. Inside the interior horizon, r_-, a ring singularity is present which, however, cannot be observed by any observer situated outside the exterior horizon. If the condition $M^2 < a^2+Q^2$ is satisfied, no horizons are present and the Kerr–Newman spacetime represents the exterior field of a naked singularity.

Despite of its fundamental importance in general relativity, and its theoretical and mathematical interest, this solution has not been especially useful for describing astrophysical phenomena, first of all, because observed astrophysical objects do not possess an appreciable net electric charge. Furthermore, the limiting Kerr metric takes into account the mass and the rotation, but does not consider the moment of inertia of the object. For astrophysi-

cal applications it is, therefore, necessary to use more general solutions with higher multipole moments which are due not only to the rotation of the body but also to its shape. This means that even in the limiting case of a static spacetime, a solution is needed that takes into account possible deviations from spherically symmetry.

4 The general static vacuum solution

In general relativity, stationary axisymmetric solutions of Einstein's equations (1) play a crucial role for the description of the gravitational field of astrophysical objects. In particular, the black hole solutions and their generalizations that include Maxwell fields are contained within this class.

This type of exact solutions has been the subject of intensive research during the past few decades. In particular, the number of know exact solutions drastically increased after Ernst (2) discovered an elegant representation of the field equations that made it possible to search for their symmetries. These studies lead finally to the development of solution generating techniques (1) which allow us to find new solutions, starting from a given seed solution. In particular, solutions with an arbitrary number of multipole moments for the mass and angular momentum were derived in (3) and used to describe the gravitational field of rotating axially symmetric distributions of mass.

The first analysis of stationary axially symmetric gravitational fields was carried out by Weyl (4) in 1917, soon after the formulation of general relativity. In particular, Weyl discovered that in the static limit the main part of the vacuum field equations reduces to a single linear differential equation. The corresponding general solution can be written in cylindrical coordinates as an infinite sum with arbitrary constant coefficients. A particular choice of the coefficients leads to the subset of asymptotically flat solutions which is the most interesting from a physical point of view. In this section we review the main properties of stationary axisymmetric gravitational fields. In particular, we show explicitly that the main field equations in vacuum can be represented as the equations of a nonlinear sigma model in which the base space is the 4-dimensional spacetime and the target space is a 2-dimensional conformally Euclidean space.

4.1 Line element and field equations

Although there exist in the literature many suitable coordinate systems, stationary axisymmetric gravitational fields are usually described in cylindric coordinates (t, ρ, z, φ). Stationarity implies that t can be chosen as the time coordinate and the metric does not depend on time, i.e. $\partial g_{\mu\nu}/\partial t = 0$. Consequently, the corresponding timelike Killing vector has the components δ^{μ}_{t}.

A second Killing vector field is associated to the axial symmetry with respect to the axis $\rho = 0$. Then, choosing φ as the azimuthal angle, the metric satisfies the conditions $\partial g_{\mu\nu}/\partial\varphi = 0$, and the components of the corresponding spacelike Killing vector are δ^{μ}_{φ}.

Using further the properties of stationarity and axial symmetry, together with the vacuum field equations, for a general metric of the form $g_{\mu\nu} = g_{\mu\nu}(\rho, z)$, it is possible to show that the most general line element for this type of gravitational fields can be written in the Weyl-Lewis-Papapetrou form as (4; 5; 6)

$$ds^2 = f(dt - \omega d\varphi)^2 - f^{-1}\left[e^{2\gamma}(d\rho^2 + dz^2) + \rho^2 d\varphi^2\right] , \tag{4.1.1}$$

where f, ω and γ are functions of ρ and z, only. After some rearrangements which include the introduction of a new function $\Omega = \Omega(\rho, z)$ by means of

$$\rho\partial_\rho\Omega = f^2\partial_z\omega , \qquad \rho\partial_z\Omega = -f^2\partial_\rho\omega , \tag{4.1.2}$$

the vacuum field equations $R_{\mu\nu} = 0$ can be shown to be equivalent to the following set of partial differential equations

$$\frac{1}{\rho}\partial_\rho(\rho\partial_\rho f) + \partial_z^2 f + \frac{1}{f}[(\partial_\rho\Omega)^2 + (\partial_z\Omega)^2 - (\partial_\rho f)^2 - (\partial_z f)^2] = 0 , \tag{4.1.3}$$

$$\frac{1}{\rho}\partial_\rho(\rho\partial_\rho\Omega) + \partial_z^2\Omega - \frac{2}{f}\left(\partial_\rho f\,\partial_\rho\Omega + \partial_z f\,\partial_z\Omega\right) = 0 , \tag{4.1.4}$$

$$\partial_\rho\gamma = \frac{\rho}{4f^2}\left[(\partial_\rho f)^2 + (\partial_\rho\Omega)^2 - (\partial_z f)^2 - (\partial_z\Omega)^2\right] , \tag{4.1.5}$$

$$\partial_z\gamma = \frac{\rho}{2f^2}\left(\partial_\rho f\,\partial_z f + \partial_\rho\Omega\,\partial_z\Omega\right) . \tag{4.1.6}$$

It is clear that the field equations for γ can be integrated by quadratures, once f and Ω are known. For this reason, the equations (4.1.3) and (4.1.4) for f and Ω are usually considered as the main field equations for stationary axisymmetric vacuum gravitational fields. In the following subsections we will focus on the analysis of the main field equations, only. It is interesting to mention that this set of equations can be geometrically interpreted in the context of nonlinear sigma models (7).

Let us consider the special case of static axisymmetric fields. This corresponds to metrics which, apart from being axially symmetric and independent of the time coordinate, are invariant with respect to the transformation $\varphi \to -\varphi$ (i.e. rotations with respect to the axis of symmetry are not allowed). Consequently, the corresponding line element is given by (4.1.1) with $\omega = 0$,

and the field equations can be written as

$$\partial_\rho^2\psi + \frac{1}{\rho}\partial_\rho\psi + \partial_z^2\psi = 0\,, \quad f = \exp(2\psi)\,, \tag{4.1.7}$$

$$\partial_\rho\gamma = \rho\left[(\partial_\rho\psi)^2 - (\partial_z\psi)^2\right]\,, \quad \partial_z\gamma = 2\rho\partial_\rho\psi\,\partial_z\psi\,. \tag{4.1.8}$$

We see that the main field equation (4.1.7) corresponds to the linear Laplace equation for the metric function ψ.

4.2 Static solution

The general solution of Laplace's equation is known and, if we demand additionally asymptotic flatness, we obtain the Weyl solution which can be written as (4; 1)

$$\psi = \sum_{n=0}^{\infty} \frac{a_n}{(\rho^2+z^2)^{\frac{n+1}{2}}} P_n(\cos\theta)\,, \qquad \cos\theta = \frac{z}{\sqrt{\rho^2+z^2}}\,, \tag{4.2.1}$$

where a_n $(n = 0, 1, ...)$ are arbitrary constants, and $P_n(\cos\theta)$ represents the Legendre polynomials of degree n. The expression for the metric function γ can be calculated by quadratures by using the set of first order differential equations (4.1.8). Then

$$\gamma = -\sum_{n,m=0}^{\infty} \frac{a_n a_m (n+1)(m+1)}{(n+m+2)(\rho^2+z^2)^{\frac{n+m+2}{2}}} \left(P_n P_m - P_{n+1}P_{m+1}\right)\,. \tag{4.2.2}$$

Since this is the most general static, axisymmetric, asymptotically flat vacuum solution, it must contain all known solution of this class. In particular, one of the most interesting special solutions which is Schwarzschild's spherically symmetric black hole spacetime must be contained in this class. To see this, we must choose the constants a_n in such a way that the infinite sum (4.2.1) converges to the Schwarzschild solution in cylindric coordinates. But, or course, this representation is not the most appropriate to analyze the interesting physical properties of Schwarzschild's metric.

In fact, it turns out that to investigate the properties of solutions with multipole moments it is more convenient to use prolate spheroidal coordinates (t, x, y, φ) in which the line element can be written as

$$ds^2 = f dt^2 - \frac{\sigma^2}{f}\left[e^{2\gamma}(x^2-y^2)\left(\frac{dx^2}{x^2-1} + \frac{dy^2}{1-y^2}\right) + (x^2-1)(1-y^2)d\varphi^2\right]$$

where

$$x = \frac{r_+ + r_-}{2\sigma}\,, \quad (x^2 \geq 1), \quad y = \frac{r_+ - r_-}{2\sigma}\,, \quad (y^2 \leq 1) \tag{4.2.3}$$

$$r_\pm^2 = \rho^2 + (z \pm \sigma)^2\,, \quad \sigma = const\,, \tag{4.2.4}$$

and the metric functions are f, ω, and γ depend on x and y, only. In this coordinate system, the general static solution which is also asymptotically flat can be expressed as

$$f = \exp(2\psi)\,, \quad \psi = \sum_{n=0}^{\infty} (-1)^{n+1} q_n P_n(y) Q_n(x)\,, \quad q_n = const$$

where $P_n(y)$ are the Legendre polynomials, and $Q_n(x)$ are the Legendre functions of second kind. In particular,

$$P_0 = 1, \quad P_1 = y, \quad P_2 = \frac{1}{2}(3y^2 - 1)\,, ...$$

$$Q_0 = \frac{1}{2}\ln\frac{x+1}{x-1}\,, \quad Q_1 = \frac{1}{2}x\ln\frac{x+1}{x-1} - 1\,,$$
$$Q_2 = \frac{1}{2}(3x^2 - 1)\ln\frac{x+1}{x-1} - \frac{3}{2}x\,, ...$$

The corresponding function γ can be calculated by quadratures and its general expression has been explicitly derived in (8). The most important special cases contained in this general solution are the Schwarzschild metric

$$\psi = -q_0 P_0(y) Q_0(x)\,, \quad \gamma = \frac{1}{2}\ln\frac{x^2-1}{x^2-y^2}\,,$$

and the Erez-Rosen metric (9)

$$\psi = -q_0 P_0(y) Q_0(x) - q_2 P_2(y) Q_2(x)\,, \quad \gamma = \frac{1}{2}\ln\frac{x^2-1}{x^2-y^2} + ...$$

In the last case, the constant parameter q_2 turns out to determine the quadrupole moment. In general, the constants q_n represent an infinite set of parameters that determines an infinite set of mass multipole moments.

5 Stationary generalization

The solution generating techniques (12) can be applied, in particular, to any static seed solution in order to obtain the corresponding stationary generalization. One of the most powerful techniques is the inverse method (ISM) developed by Belinski and Zakharov (13). We used a particular case of the ISM, which is known as the Hoenselaers–Kinnersley-Xanthopoulos (HKX) transformation to derive the stationary generalization of the general static solution in prolate spheroidal coordinates.

5.1 Ernst representation

In the general stationary case ($\omega \neq 0$) with line element

$$\begin{aligned} & ds^2 = f(dt - \omega d\varphi)^2 \\ - \quad & \frac{\sigma^2}{f}\left[e^{2\gamma}(x^2-y^2)\left(\frac{dx^2}{x^2-1}+\frac{dy^2}{1-y^2}\right)+(x^2-1)(1-y^2)d\varphi^2\right] \end{aligned}$$

it is useful to introduce the the Ernst potentials

$$E = f + i\Omega\,, \quad \xi = \frac{1-E}{1+E}\,,$$

where the function Ω is now determined by the equations

$$\sigma(x^2-1)\Omega_x = f^2\omega_y\,, \quad \sigma(1-y^2)\Omega_y = -f^2\omega_x\,.$$

Then, the main field equations can be represented in a compact and symmetric form:

$$(\xi\xi^*-1)\left\{[(x^2-1)\xi_x]_x + [(1-y^2)\xi_y]_y\right\} = 2\xi^*[(x^2-1)\xi_x^2 + (1-y^2)\xi_y^2]\,.$$

This equation is invariant with respect to the transformation $x \leftrightarrow y$. Then, since the particular solution

$$\xi = \frac{1}{x} \to \Omega = 0 \to \omega = 0 \to \gamma = \frac{1}{2}\ln\frac{x^2-1}{x^2-y^2}$$

represents the Schwarzschild spacetime, the choice $\xi^{-1} = y$ is also an exact solution. Furthermore, if we take the linear combination $\xi^{-1} = c_1 x + c_2 y$ and introduce it into the field equation, we obtain the new solution

$$\xi^{-1} = \frac{\sigma}{M} x + i \frac{a}{M} y \, , \; \sigma = \sqrt{M^2 - a^2} \, ,$$

which corresponds to the Kerr metric in prolate spheroidal coordinates.

In the case of the Einstein-Maxwell theory, the main field equations can be expressed as

$$(\xi\xi^* - \mathcal{F}\mathcal{F}^* - 1)\nabla^2\xi = 2(\xi^*\nabla\xi - \mathcal{F}^*\nabla\mathcal{F})\nabla\xi \, ,$$

$$(\xi\xi^* - \mathcal{F}\mathcal{F}^* - 1)\nabla^2\mathcal{F} = 2(\xi^*\nabla\xi - \mathcal{F}^*\nabla\mathcal{F})\nabla\mathcal{F}$$

where ∇ represents the gradient operator in prolate spheroidal coordinates. Moreover, the gravitational potential ξ and the electromagnetic $\mathcal{F}$ Ernst potential are defined as

$$\xi = \frac{1 - f - i\Omega}{1 + f + i\Omega} \, , \quad \mathcal{F} = 2\frac{\Phi}{1 + f + i\Omega} \, .$$

The potential Φ can be shown to be determined uniquely by the electromagnetic potentials A_t and A_φ One can show that if ξ_0 is a vacuum solution, then the new potential

$$\xi = \xi_0 \sqrt{1 - e^2}$$

represents a solution of the Einstein-Maxwell equations with effective electric charge e. This transformation is known in the literature as the Harrison transformation (10). Accordingly, the Kerr–Newman solution in this representation acquires the simple form

$$\xi = \frac{\sqrt{1 - e^2}}{\frac{\sigma}{M} x + i \frac{a}{M} y} \, , \qquad e = \frac{Q}{M} \, , \qquad \sigma = \sqrt{M^2 - a^2 - Q^2} \, .$$

In this way, it is very easy to generalize any vacuum solution to include the case of electric charge. More general transformations of this type can be used in order to generate solutions with any desired set of gravitational and electromagnetic multipole moments (11).

5.2 The general solution

If we take as seed metric the general static solution, the application of two HXK transformations generates a stationary solution with an infinite number of gravitoelectric and gravitomagnetic multipole moments. The HKX method is applied at the level of the Ernst potential from which the metric functions

can be calculated by using the definition of the Ernst potential E and the field equations for γ. The resulting expressions in the general case are quite cumbersome. We quote here only the special case in which only an arbitrary quadrupole parameter is present. In this case, the result can be written as

$$\begin{aligned} f &= \frac{R}{L} e^{-2qP_2Q_2} , \\ \omega &= -2a - 2\sigma \frac{\mathcal{M}}{R} e^{2qP_2Q_2} , \\ e^{2\gamma} &= \frac{1}{4}\left(1+\frac{M}{\sigma}\right)^2 \frac{R}{x^2-y^2} e^{2\hat{\gamma}} , \end{aligned} \tag{5.2.1}$$

where

$$\begin{aligned} R &= a_+a_- + b_+b_- , \qquad L = a_+^2 + b_+^2 , \\ \mathcal{M} &= \alpha x(1-y^2)(e^{2q\delta_+} + e^{2q\delta_-})a_+ + y(x^2-1)(1-\alpha^2 e^{2q(\delta_+ + \delta_-)})b_+ , \\ \hat{\gamma} &= \frac{1}{2}(1+q)^2 \ln\frac{x^2-1}{x^2-y^2} + 2q(1-P_2)Q_1 + q^2(1-P_2)\Big[(1+P_2)(Q_1^2-Q_2^2) \\ &\quad + \frac{1}{2}(x^2-1)(2Q_2^2 - 3xQ_1Q_2 + 3Q_0Q_2 - Q_2')\Big] . \end{aligned} \tag{5.2.2}$$

Here $P_l(y)$ and $Q_l(x)$ are Legendre polynomials of the first and second kind respectively. Furthermore

$$\begin{aligned} a_\pm &= x(1-\alpha^2 e^{2q(\delta_+ + \delta_-)}) \pm (1+\alpha^2 e^{2q(\delta_+ + \delta_-)}) , \\ b_\pm &= \alpha y(e^{2q\delta_+} + e^{2q\delta_-}) \mp \alpha(e^{2q\delta_+} - e^{2q\delta_-}) , \\ \delta_\pm &= \frac{1}{2}\ln\frac{(x\pm y)^2}{x^2-1} + \frac{3}{2}(1-y^2 \mp xy) + \frac{3}{4}[x(1-y^2) \mp y(x^2-1)]\ln\frac{x-1}{x+1} , \end{aligned}$$

the quantity α being a constant

$$\alpha = \frac{\sigma - M}{a} , \qquad \sigma = \sqrt{M^2 - a^2} . \tag{5.2.3}$$

The physical significance of the parameters entering this metric can be clarified by calculating the Geroch-Hansen (14; 15) multipole moments

$$M_{2k+1} = J_{2k} = 0 , \quad k = 0, 1, 2, ... \tag{5.2.4}$$

$$M_0 = M , \quad M_2 = -Ma^2 + \frac{2}{15} qM^3 \left(1 - \frac{a^2}{M^2}\right)^{3/2} , ... \tag{5.2.5}$$

$$J_1 = Ma , \quad J_3 = -Ma^3 + \frac{4}{15} qM^3 a \left(1 - \frac{a^2}{M^2}\right)^{3/2} , ... \tag{5.2.6}$$

The vanishing of the odd gravitoelectric (M_n) and even gravitomagnetic (J_n) multipole moments is a consequence of the symmetry with respect to the equatorial plane. From the above expressions we see that M is the total mass of the body, a represents the specific angular momentum, and q is related to the deviation from spherical symmetry. All higher multipole moments can be shown to depend only on the parameters M, a, and q.

We analyzed the geometric and physical properties of the above solution. The special cases contained in the general solution suggest that it can be used to describe the exterior asymptotically flat gravitational field of rotating body with arbitrary quadrupole moment. This is confirmed by the analysis of the motion of particles on the equatorial plane. The quadrupole moment turns out to drastically change the geometric structure of spacetime as well as the motion of particles, especially near the gravitational source.

We investigated in detail the properties of the Quevedo-Mashhoon (QM) spacetime which is a generalization of Kerr spacetime, including an arbitrary quadrupole. Our results show (16) that a deviation from spherical symmetry, corresponding to a non-zero electric quadrupole, completely changes the structure of spacetime. A similar behavior has been found in the case of the Erez-Rosen spacetime. In fact, a naked singularity appears that affects the ergosphere and introduces regions where closed timelike curves are allowed. Whereas in the Kerr spacetime the ergosphere corresponds to the boundary of a simply-connected region of spacetime, in the present case the ergosphere is distorted by the presence of the quadrupole and can even become transformed into non simply-connected regions. All these changes occur near the naked singularity which is situated at $x = 1$, a value that corresponds to the radial distance $r = M + \sqrt{M^2 - a^2}$ in Boyer-Lindquist coordinates. In the limiting case $a/M > 1$, the multipole moments and the metric become complex, indicating that the physical description breaks down. Consequently, the extreme Kerr black hole represents the limit of applicability of the QM spacetime.

Since standard astrophysical objects satisfy the condition $a/M < 1$, we can conclude that the QM metric can be used to describe their exterior gravitational field. Two alternative situations are possible. If the characteristic radius of the body is greater than the critical distance $M + \sqrt{M^2 - a^2}$, i.e. $x > 1$, the exterior solution must be matched with an interior solution in order to describe the entire spacetime. If, however, the characteristic radius of the body is smaller than the critical distance $M + \sqrt{M^2 - a^2}$, the QM metric describes the field of a naked singularity.

The presence of a naked singularity leads to interesting consequences in the motion of test particles. For instance, repulsive effects can take place in a region very closed to the naked singularity. In that region stable circular orbits can exist. The limiting case of static particle is also allowed. Due to the complexity of the above solution, the investigation of naked singularities

can be performed only numerically. To illustrate the effects of repulsive gravity analytically, we used the simplest possible case which corresponds to the Reissner-Nordström spacetime.

6 Circular motion in the Reissner-Nordström spacetime

In general relativity, the gravitational field of a static, spherically symmetric, charged body with mass M and charge Q is described by the Reissner-Nordström metric which in standard spherical coordinates can be expressed as

$$ds^2 = -\frac{\Delta}{r^2}dt^2 + \frac{r^2}{\Delta}dr^2 + r^2\left(d\theta^2 + \sin^2\theta d\phi^2\right) , \tag{6.0.1}$$

where $\Delta = r^2 - 2Mr + Q^2$. The horizons are situated at $r_\pm = M \pm \sqrt{M^2 - Q^2}$. The study of the motion of test particles in this gravitational field is simplified by the fact that the equatorial plane, $\theta = \pi/2$, is a geodesic plane.

The tangent u^a vector to a curve $x^\alpha(\tau)$ is $u^\alpha = dx^\alpha/d\tau = \dot{x}^\alpha$, where τ is an affine parameter along the curve. The momentum $p^\alpha = \mu\dot{x}^\alpha$ of a particle with mass μ can be normalized so that $g_{\alpha\beta}\dot{x}^\alpha\dot{x}^\beta = -k$, where $k = 0, 1, -1$ for null, timelike, and spacelike curves, respectively. For the Reissner-Nordström metric we obtain

$$-\frac{\Delta}{r^2}\dot{t}^2 + \frac{r^2}{\Delta}\dot{r}^2 + r^2\dot{\phi}^2 = -k \tag{6.0.2}$$

on the equatorial plane. The last equation reduces to a first-order differential equation

$$-\frac{E^2r^2}{\mu^2\Delta} + \frac{r^2}{\Delta}\dot{r}^2 + \frac{L^2}{\mu^2r^2} = -k\,, \tag{6.0.3}$$

where we have used the expressions for the energy $E \equiv -g_{\alpha\beta}\xi_t^\alpha p^\beta = \mu\frac{\Delta}{r^2}\dot{t}$, and angular momentum $L \equiv g_{\alpha\beta}\xi_\phi^\alpha p^\beta = \mu r^2\dot{\phi}$ of the test particle, which are constants of motion associated with the Killing vector fields $\xi_t = \partial_t$ and $\xi_\phi = \partial_\phi$, respectively. Equation (6.0.3) can be rewritten as

$$\dot{r}^2 + V^2 = \frac{E^2}{\mu^2}\,, \quad \text{with} \quad V \equiv \sqrt{\left(k + \frac{L^2}{\mu^2r^2}\right)\left(1 - \frac{2M}{r} + \frac{Q^2}{r^2}\right)}\,. \tag{6.0.4}$$

The investigation of the motion of test particles in the gravitational field of the Reissner-Nordström metric is thus reduced to the study of motion in the effective potential V. In this work, we will focus mainly on circular orbits for which $\dot{r} = 0$ and $V = E/\mu$, with the condition $\partial V/\partial r = 0$. A straightforward

calculation shows that this condition leads to

$$\frac{L^2}{\mu^2} = k\frac{r^2(Mr - Q^2)}{r^2 - 3Mr + 2Q^2}\,, \tag{6.0.5}$$

an expression which we substitute in Eq.(6.0.4) to obtain

$$\frac{E^2}{\mu^2} = k\frac{(r^2 - 2Mr + Q^2)^2}{r^2(r^2 - 3Mr + 2Q^2)}\,. \tag{6.0.6}$$

Moreover, from the physical viewpoint it is important to find the minimum radius for stable circular orbits which is determined by the inflection points of the effective potential function, i.e., by the equation $\partial^2 V/\partial^2 r = 0$. It is easy to show that for the potential (6.0.4), the last equation is equivalent to

$$Mr^3 - 6M^2r^2 + 9MQ^2r - 4Q^4 = 0\,. \tag{6.0.7}$$

We performed a detailed analysis of the circular motion of test particles governed by the above equations. Since the behavior of test particles strongly depends on the ratio Q/M, it is necessary to consider separately the cases of black holes ($Q/M < 1$), extreme black holes ($Q/M = 1$) and naked singularities ($Q/M > 1$).

6.1 Black holes

From the expressions for the energy and angular momentum of a timelike particle ($k = 1$) one sees that motion is possible only for $r > Q^2/M = r_*$ and for $r^2 - 3Mr + 2Q^2 > 0$. i. e. $r < r_{\gamma_-}$ and $r > r_{\gamma_+}$, with $r_{\gamma_\pm} \equiv [3M \pm \sqrt{(9M^2 - 8Q^2)}]/2$. In fact, from Eqs.(6.0.5) and (6.0.6) it follows that the motion inside the regions $r < r_*$ and $r \in (r_{\gamma_-}, r_{\gamma_+})$ is possible only along spacelike geodesics. At $r = r_{\gamma_\pm}$ one finds instead that the velocity of test particles at $v_{g_+} = 1$ must be equal to the velocity of light, i.e., the circles $r = r_{\gamma_\pm}$ represent null hypersurface.

At infinity, the effective potential tends to a constant which is independent of the value of the parameters of the test particle and of the gravitational source. In our case, we have normalized this constant by choosing the value of the total energy of the particle as E/μ. Moreover, as the outer horizon is approached from outside, the effective potential reaches its global minimum value and vanishes. The radius of circular orbits, $r_{\rm CO}$, is determined by the real positive root of the equation

$$Mr^3 - \left(Q^2 + \frac{L^2}{\mu^2}\right)r^2 + \frac{3ML^2}{\mu^2}r - \frac{2Q^2L^2}{\mu^2} = 0\,. \tag{6.1.1}$$

In general, in the region $r > r_{\gamma+}$ circular orbits do not always exist. For instance, for $Q = 0$ no circular orbits exist for $|L/(\mu M)| < \sqrt{12} \approx 3.45$, whereas for $Q = M$ and $Q = 0.5M$ the existence condition implies that $|L/(\mu M)| < \sqrt{8} \approx 2.83$ and $|L/(\mu M)| < 3.33774$, respectively.

In this context, it is interesting to explore the stability properties of the circular motion at $r = r_{\rm CO}$. To find the explicit value of the last stable radius we solve the condition (6.0.7) in the black hole region and find

$$\frac{r_{\rm LSCO}}{M} = 2 + \frac{4 - \frac{3Q^2}{M^2} + \left[8 + \frac{2Q^4}{M^4} + \frac{Q^2\left(-9+\sqrt{5-\frac{9Q^2}{M^2}+\frac{4Q^4}{M^4}}\right)}{M^2}\right]^{2/3}}{\left[8 + \frac{2Q^4}{M^4} + \frac{Q^2\left(-9+\sqrt{5-\frac{9Q^2}{M^2}+\frac{4Q^4}{M^4}}\right)}{M^2}\right]^{1/3}} . \tag{6.1.2}$$

As expected, in the limiting case $Q \to 0$, we obtain the Schwarzschild value $r^{\rm max}_{\rm LSCO} = 6M$. The value of $r_{\rm LSCO}$ decreases as Q/M increases, until it reaches its minimum value $r^{\rm min}_{\rm LSCO} = 4M$ at $Q/M = 1$.

Orbits with $r > r_{\rm LSCO}$ are stable, whereas the circular motion in the region $r_{\gamma_+} < r < r_{\rm LSCO}$ is completely unstable. Since the velocity of a test particle at $r = r_{\gamma_+}$ must equal the velocity of light, one can expect that a particle in the unstable region will reach very rapidly the orbit at $r = r_{\rm LSCO}$. For a static observer inside the unstable region, the hypersurface $r = r_{\gamma_+}$ might appear as a source of "repulsive gravity". This intuitive result can be corroborated by analyzing the behavior of energy and angular momentum of test particles. Both quantities diverge as the limiting radius $r = r_{\gamma_+}$ is approached, indicating that an infinite amount of energy and angular momentum is necessary to reach $r = r_{\gamma_+}$. As the ratio Q/M increases, the values of the energy and angular momentum at the last stable orbit decrease. For large values of the radius, the energy of circular orbits approaches the limit $E = \mu$, and the angular momentum $L/(M\mu)$ increases monotonically.

As a general result we obtain that the values for the radius of the last stable orbit as well as of the corresponding energy and angular momentum diminish due to the presence of the electric charge. Physically, this means that the additional gravitational field generated by the electric charge acts on neutral particles as an additional attractive force which reduces the radius of the last stable orbit.

6.2 Extreme black holes

In the case of an extreme black hole ($Q = M$) the outer and inner horizons coincide at $r_{\pm} = M$. The effective potential vanishes at the horizon and tends to 1 as spatial infinity is approached. In this open interval no divergencies are observed. The effective potential reduces to

$$V = \sqrt{1 + \frac{L^2}{\mu^2 r^2}} \left(1 - \frac{M}{r}\right) . \tag{6.2.1}$$

so that the radius of circular orbits is

$$\frac{r_{\text{CO}}}{M} = \frac{L^2 - L\sqrt{-8\mu^2 M^2 + L^2}}{2\mu^2 M^2} \tag{6.2.2}$$

The energy and angular momentum of test particles moving along circular orbits are given by

$$\frac{E^2}{\mu^2} = \frac{(r-M)^3}{r^2(r-2M)}, \qquad \frac{L^2}{\mu^2} = \frac{Mr^2}{r-2M} . \tag{6.2.3}$$

Consequently, timelike circular orbits are restricted by the condition $r > r_{g+} = 2M$. As $r \to 2M$, the energy and angular momentum diverge, indicating that the circular motion at r_{γ_+} is possible only along null geodesics. As expected, the local minimum of these graphics determine the radius of the last stable orbit. At $r = r_{\text{LSCO}}$, the energy is $E \approx 0.918\mu$ and the angular momentum $L = 2\sqrt{2}\mu M$.

In general, we can see that this limiting case is very similar to the case of an arbitrary black hole. The radius of the last stable circular orbits reaches its minimum value, $r^{\text{min}}_{\text{LSCO}} = 4M$, for a black hole, and the energy and angular momentum of the test particle diminishes as the minimum radius is approached.

6.3 Naked singularities

In the naked singularity case, $Q > M$, an inspection of the values for the energy and angular momentum

$$\frac{E}{\mu} = \frac{Q^2 + (r-2M)r}{r\sqrt{2Q^2 + (r-3M)r}}, \quad \frac{L_+}{(\mu M)} = \frac{r}{M}\sqrt{\frac{rM - Q^2}{2Q^2 - 3Mr + r^2}} . \tag{6.3.1}$$

of the test particle shows that it is necessary to study separately four different regions: the region $1 < Q^2/M^2 < 9/8$, the value $Q^2 = \frac{9}{8}M^2$, the region $Q^2/M^2 > 9/8$ and finally the value $r = Q^2/M$.

The main results obtained from the study of the black hole and naked singularity cases are here summarized and compared in the plots of Fig.(6.1–6.3). In the three-dimensional plots of Fig.6.1 the energy and the angular momentum (6.0.6) are shown as functions of the circular orbits radius and the ratio Q/M, for both black hole and naked singularity cases.

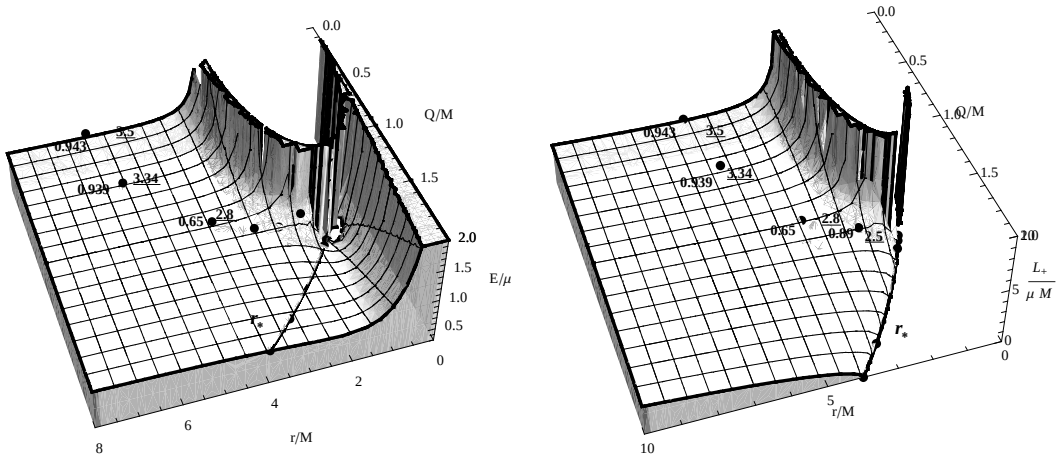

Figure 6.1: The pictures show the energy E/μ *(a)*, and the angular momentum $L_+/(\mu M)$ *(b)*, of a circular orbit for a neutral particle of mass μ in a Reissner-Nordström geometry of charge Q and mass M as function of r/M and charge-mass ratio Q/M in the range $[0, 2]$. The $r = r_* \equiv Q^2/M$ line is also plotted. Numbers close to the points sign the energy and the angular momentum (underlined numbers) of the last stable circular orbits.

Fig.6.2 shows the circular orbits radius as a function of the angular momentum for black hole as well as for naked singularity configurations. One can see that the value of the central charge affects very drastically the motion of test particles. A naked singularity presents a very peculiar behavior due to the appearance of regions in which repulsive gravity plays an important role and even dominates over attractive gravity, for some values of the central charge. In Fig.6.2, the limiting Schwarzschild and Newtonian cases are also included for the sake of generality. It can be seen that for large values of r/M the radius approaches the Schwarzschild and Newtonian limiting cases. This is in agreement with the fact that asymptotically the mass term dominates over the charge term and that far away from the source the effective potential approaches the Newtonian gravitational potential.

Finally, the study of the stability of circular orbits is summarized in the Fig.6.3 where the radius of the last stable circular orbits is plotted as a function of the charge-to-mass ratio Q/M. We see that the location and structure of the stability zones of neutral particles around a black differs in a very strong way from the case of a naked singularity. In the case of a black hole, it is possible to find a stable circular orbit for any radius value greater that the value of the last stable orbit.

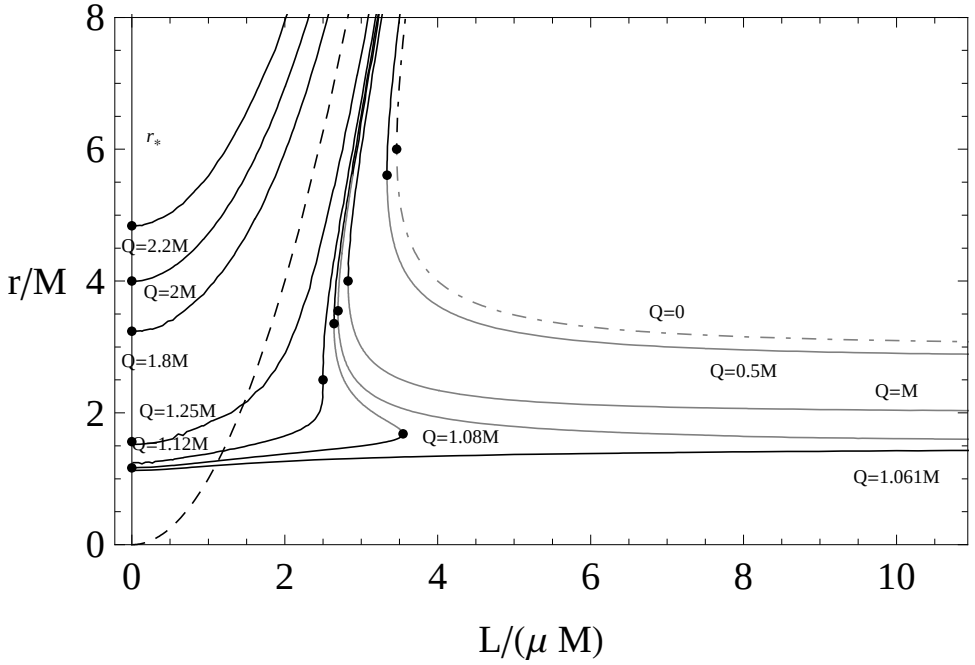

Figure 6.2: The radius r/M of circular orbits for a neutral particle of mass μ in a Reissner-Nordström spacetime, with charge Q and mass M, is plotted as a function of the angular momentum $L/(\mu M)$ for different values of the ratio Q/M in the interval $[0, 2]$. The radius of circular orbits for the Newtonian limit (dashed line) and the radius of the circular orbits for Schwarzschild case (dot-dashed line) are also plotted. The points represent the last circular orbits. Black-lines represent stable circular orbits, gray-lines represent unstable circular orbits. The curve $r = r_* \equiv Q^2/M$ is also plotted for comparison.

If we assume that test particles on circular motion around a black can be considered as being the constituents of an accretion disk, we conclude that such an accretion disk presents a continuous structure with a minimum radius which coincides with the radius of the last stable circular orbit. Accordingly, the minimum radius of such a hypothetical accretion disk is equal to $4M$ in the case of an extreme black hole, whereas the maximum radius value of $6M$ is reached in the case of the Schwarzschild black hole with vanishing charge.

In the case of a naked singularity configuration, the situation is completely different. Fig.6.4 represents this particular case in more detail. The main difference consists now in the possible structure of an accretion disk. Indeed, we see that in the open interval $1 < Q^2/M^2 < 9/8$, two zones of stability are possible, namely, in the interval (r_*, r_{c-}) and in the region $r > r_{c+}$. This means that an accretion disk in this region must have a discontinuous structure. In fact, particles can move on stable circular orbits in the interval (r_*, r_{c-}) which determines the interior and the exterior radius of the first accretion disk with a ring-like structure. In the region $r > r_{c+}$ a second disk can exist with interior radius r_{c+}. This structure is schematically illustrated in Fig. 6.5. A more

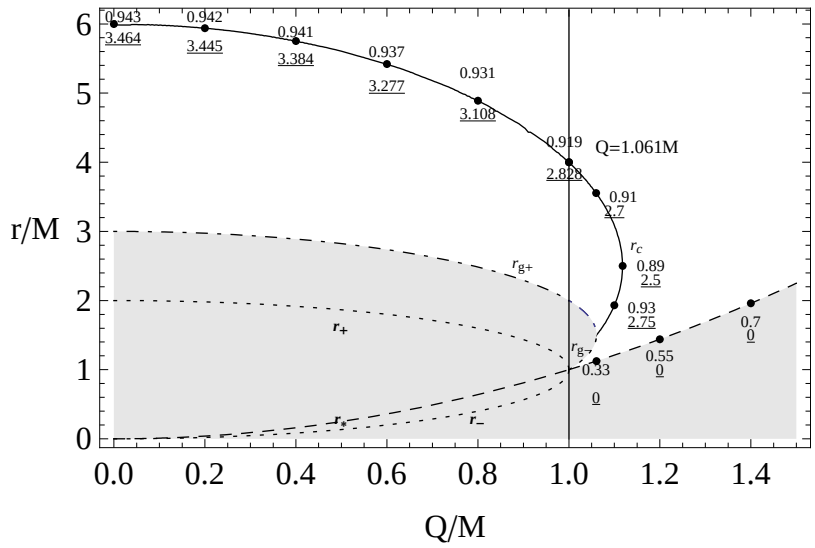

Figure 6.3: The minimum radius r/M for a stable circular orbit of a neutral particle of mass μ in a Reissner-Nordström geometry of charge Q and mass M is plotted as a function of Q/M. The ratio Q/M varies in the interval $[0, 1.5]$; in particular, for $Q = 0$ we find $r = 6M$ with $r_+ \equiv 2M$ and $r_{\gamma_+} = 3M$, for $Q = 1$ we find $r = 4M$ with $r_+ = M$ and $r_{\gamma_+} = 2M$. Here, $r_{\gamma_+} \equiv [3M + \sqrt{(9M^2 - 8Q^2)}]/2$ and $r_+ \equiv M + \sqrt{M^2 - Q^2}$. Numbers close to the points represent the energy E/μ and the angular momentum $L/(\mu M)$ (underlined numbers) of the last stable circular orbits.

detailed analysis will be necessary in order to establish whether this discontinuous structure of an accretion disk around a naked singularity can lead to observable effects.

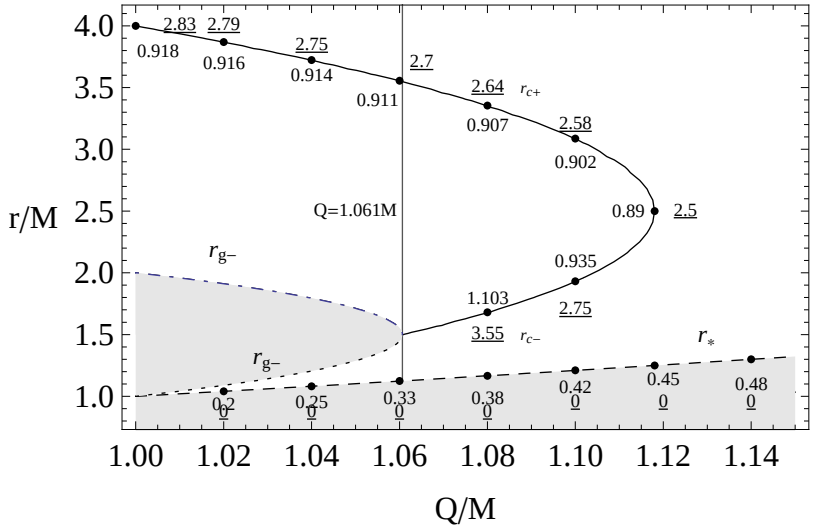

Figure 6.4: The minimum radius (black line) for the last stable circular orbit of a neutral particle of mass μ in a Reissner-Nordström naked singularity of charge Q and mass M is plotted as a function of the ratio Q/M in the interval $[1, 2.2]$. The dashed curve represents $r \equiv r_* = Q^2/M$, the dotted curve is $r = r_{\gamma_-} \equiv [3M - \sqrt{(9M^2 - 8Q^2)}]/2$, while the dot-dashed curve is $r = r_{\gamma_+} \equiv [3M + \sqrt{(9M^2 - 8Q^2)}]/2$. The shaded regions are forbidden, for $1 < Q/M < 1.061$ circular orbits can exist only for $r_* < r < r_{\gamma_-}$ (all stable) and $r > r_{\gamma_+}$ (unstable in $r_{\gamma_+} < r < r_c$, stable for $r > r_c$), while for $Q/M > 1.061$ circular orbits can exist only for $r > r_*$. The effective potential has a minimum in $r \equiv r_*$ where $L/(\mu M)(r_*) = 0$. Numbers close to the points sign the energy E/μ and the angular momentum $L/(\mu M)$ (underlined numbers) of the last stable circular orbits.

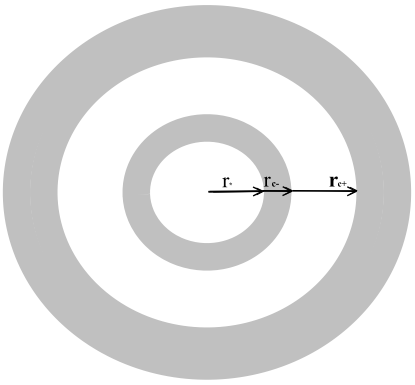

Figure 6.5: Structure of an accretion disk around a naked singularity. The interior ring is situated within the interior region of stability.

7 Toward an invariant definition of repulsive gravity

It is well known that the field equations of Einstein's theory of gravity allow the existence of exact solutions containing naked singularities. In fact, in this report we have mentioned several times that such solutions are contained as special cases in the QM class of solutions.

Moreover, recent studies indicate that under certain circumstances naked singularities can appear as the result of a realistic gravitational collapse (38). An intriguing property of many naked singularities is that they can generate repulsive gravity. To understand this repulsive nature one can study the motion of test particles which, for example in the case of stationary axially symmetric fields, reduces to the study of an effective potential. Although the explicit form of the effective potential depends on the type of motion under consideration, in general one can find certain similitudes between the effective potential for geodesic motion and the effective Newtonian potential which follows from the metric as $g_{tt} \approx 1 - 2V_N = 1 - 2M_{eff}/r$, where the effective mass reduces to the physical mass M at infinity. One can then intuitively expect that in the regions where M_{eff} becomes negative, the effects of repulsive gravity may occur. In the case of the Schwarzschild metric the effective mass coincides with the physical mass, and repulsive gravity is obtained only if we change $M \to -M$; hence, the source of repulsion can be considered as unphysical. However, in the cases of the Reissner-Nordström and Kerr metrics we have respectively $M_{eff} = M - \frac{Q}{2r}$ and $M_{eff} = M - L(a, r, \theta)$,(47) leading to spacetime regions where repulsive gravity exists. The disadvantage of this approach is that it is clearly coordinate and observer dependent. The attempts to define gravitational repulsion in terms of curvature invariants (39) and the behavior of light cones (40) are also not definite. In this work we propose to use the eigenvalues of the curvature tensor to characterize repulsive gravity in an invariant manner. We first consider the main second order curvature invariants and show that they do not reproduce the simple case of the Schwarzschild naked singularity. Then we show that the curvature eigenvalues provide a reasonable solution to the problem.

7.1 An invariant approach

From the curvature tensor one can form 14 functionally independent scalars of which only 4 are non-zero in empty space (48). As for the second order invariants, the most interesting are the Kretschmann scalar, $K_1 = R_{\alpha\beta\gamma\delta}R^{\alpha\beta\gamma\delta}$, the Chern-Pontryagin scalar, $K_2 = [^*R]_{\alpha\beta\gamma\delta}R^{\alpha\beta\gamma\delta}$, and the Euler scalar $K_3 = [^*R^*]_{\alpha\beta\gamma\delta}R^{\alpha\beta\gamma\delta}$, where the asterisk represents dual conjugation. Although the use of these invariants has been proposed to define "repulsive domains" and negative effective masses in curved spacetimes (39), their quadratic structure does not allow to consider all possible cases of naked singularities. Indeed, for the Schwarzschild spacetime we get $K_1 = 48M^2/r^6$, whereas K_2 and K_3 are proportional to K_1. Since the change $M \to -M$ does affect the behavior of K_1, these invariants do not recognize the presence of a Schwarzschild naked singularity. Similar difficulties appear in more general cases like the Kerr and Kerr-Newman naked singularities (41). Therefore, it seems necessary to consider the only first order invariant which is the curvature scalar R; however, it vanishes identically in the empty space of naked singularities.

As an alternative approach we propose to use the eigenvalues of the curvature. To this end, consider the $SO(3,C)-$representation of the curvature as follows. Let the line element be written in an (pseudo-)orthonormal frame as

$$ds^2 = \eta_{ab}\vartheta^a \otimes \vartheta^b \tag{7.1.1}$$

with $\eta_{ab} = \mathrm{diag}(+1,-1,-1,-1)$. From the curvature 2-form

$$\Omega^a{}_b = d\omega^a{}_b + \omega^a{}_c \wedge \omega^c{}_b = \frac{1}{2}R^a{}_{bcd}\vartheta^c \wedge \vartheta^d \,, \tag{7.1.2}$$

where $d\vartheta^a = -\omega^a{}_b \wedge \vartheta^b$, one obtains the components of the curvature tensor whose irreducible parts are: the Weyl tensor,

$$W_{abcd} = R_{abcd} + 2\eta_{[a|[c}R_{d]|b]} + \frac{1}{6}R\eta_{a[d}\eta_{c]b} \,, \tag{7.1.3}$$

the trace-free Ricci tensor,

$$E_{abcd} = 2\eta_{[b|[c}R_{d]|a]} - \frac{1}{2}R\eta_{a[d}\eta_{c]b} \,, \tag{7.1.4}$$

and the curvature scalar,

$$S_{abcd} = -\frac{1}{6}R\eta_{a[d}\eta_{c]b} \,, \tag{7.1.5}$$

with $R_{ab} = \eta^{cd}R_{cabd}$. Furthermore, using the bivector notation for the indices $ab \to A$, according to $01 \to 1,\ 02 \to 2,\ 03 \to 3,\ 23 \to 4,\ 31 \to 5,\ 12 \to 6$, the

curvature tensor can be written as $R_{AB} = W_{AB} + E_{AB} + S_{AB}$ with

$$W_{AB} = \begin{pmatrix} N & M \\ M & -N \end{pmatrix}, E_{AB} = \begin{pmatrix} P & Q \\ Q & -P \end{pmatrix}, S_{AB} = \frac{R}{12}\begin{pmatrix} I_3 & 0 \\ 0 & I_3 \end{pmatrix}. \quad (7.1.6)$$

Here M, N and P are (3×3) real symmetric matrices, whereas Q is antisymmetric. The $SO(3,C)-$representation corresponds to $\mathbf{R} = W + E + S$ with $W = M + iN$, $E = P + iQ$, and $S = \frac{1}{12} R\, I_3$ (see (49) for more details.) The eigenvalues of the curvature matrix $\mathbf{R}$ are in general complex $\lambda_n = a_n + ib_n$ and, according to Petrov's classification (1), are an invariant characterization of the curvature tensor. Moreover, in the most general case of gravitational fields belonging to Petrov's class I, we obtain the largest number of eigenvalues, namely $n = 3$.

In the special case of the Schwarzschild metric there is only one eigenvalue $\lambda = M/r^3$ and the change $M \to -M$ induces a drastic change in the eigenvalue and in the structure of spacetime as well. An analysis of the more general Kerr-Newman naked singularity indicates that in fact the curvature eigenvalues change their sign and present several maxima and minima in the vicinity of the singularity which is exactly the region where repulsive gravity appears. It then seems reasonable to introduce the concept of region of repulsion as the region of spacetime contained between the first extremum of the eigenvalue, when approaching from spatial infinity, and the singularity. The extremum is defined in an invariant manner as $\partial\lambda_n/\partial x^i = 0$, where x^i are the spatial coordinates. This invariant approach leads to the following values for the Reissner-Nordström and Kerr naked singularities

$$R^{RN}_{rep} = 2\frac{Q^2}{M}\,, \qquad R^{K}_{rep} = \left(1 + \sqrt{2}\right) a\cos\theta\,, \quad (7.1.7)$$

respectively. These results are in agreement with the analysis of test particles. In fact, the Reissner-Nordström singularity presents repulsion effects outside the classical radius $R_{class} = Q^2/M$, and the radius of repulsion $R^{RN}_{rep} = 2R_{class}$ is always situated within the zone of instability of circular motion. The Kerr naked singularity turns out to be attractive only on the equatorial plane $[R^{K}_{rep}(\pi/2) = 0]$, and it is repulsive otherwise. The case of the Kerr-Newman singularity cannot be solved analytically in a compact form. On the axis, however, the radius of repulsion is given by the largest root of the equation

$$Mr^4 - 2Q^2r^3 + 2a^2Q^2r - 6Ma^2r^2 + Ma^4 = 0\,. \quad (7.1.8)$$

Introducing values for the mass, charge and angular momentum the resulting radius of repulsion is always situated in the region where the motion of test particles is affected by repulsive gravity.

Our invariant approach to define repulsive gravity leads to plausible and

physical reasonable results in the case of naked singularities which possess a black hole counterpart. The investigation of naked singularities generated by a mass quadrupole moment (without black hole counterparts) indicates that our method consistently delivers the expected results. Moreover, it turns out that the concept of region of repulsion can be used as a criterion to study the problem of matching interior and exterior solutions of Einstein's equations.

8 Geometric and physical effects of the gravitational quadrupole

The problem of describing the gravitational field of astrophysical bodies is of central importance in general relativity, both as an issue of principle and as a foundation for explaining the results of observations. It is an issue of principle because general relativity is believed to be the most accurate theory of the gravitational field. Consequently, Einstein's theory should accept the existence of exact solutions that correctly describe the gravitational field of realistic sources. On the other hand, the explanation of effects observed at the astrophysical level is extremely important.

Astrophysical bodies are characterized in general by a non-spherically symmetric distribution of mass. In many cases, like ordinary planets and satellites, it is possible to neglect the deviations from spherical symmetry; it seems instead reasonable to expect that deviations should be taken into account in case of strong gravitational fields.

The general metric describing the gravitational field of a rotating deformed mass was found in 1991 by Quevedo and Mashhoon and involves an infinite set of gravitoelectric and gravitomagnetic multipoles. This is a stationary axisymmetric solution of the vacuum Einstein's equations belonging to the class of Weyl-Lewis-Papapetrou and is characterized, in general, by the presence of a naked singularity. To capture the main properties of the general solution, we concentrate for the sake of simplicity on the special case of the general solution that involves only three parameters: the mass M, the angular momentum per unit mass a and the mass quadrupole parameter q of the source. This special case was first found by Quevedo and Mashhoon in 1985. Hereafter this solution will be denoted as the QM solution.

The corresponding line element in prolate spheroidal coordinates (t, x, y, ϕ) with $x \geq 1$, $-1 \leq y \leq 1$ is given by

$$\begin{aligned} \mathrm{d}s^2 &= -f(\mathrm{d}t - \omega \mathrm{d}\phi)^2 \\ &\quad + \frac{\sigma^2}{f}\left\{ e^{2\gamma}\left(x^2 - y^2\right)\left(\frac{\mathrm{d}x^2}{x^2-1} + \frac{\mathrm{d}y^2}{1-y^2}\right) + (x^2-1)(1-y^2)\mathrm{d}\phi^2 \right\}, \end{aligned} \tag{8.0.1}$$

where f, ω and γ are functions of x and y only and σ is a constant. They have

the form

$$\begin{aligned} f &= \frac{R}{L}e^{-2qP_2Q_2}\,, \\ \omega &= -2a - 2\sigma\frac{\mathfrak{M}}{R}e^{2qP_2Q_2}\,, \\ e^{2\gamma} &= \frac{1}{4}\left(1+\frac{M}{\sigma}\right)^2\frac{R}{x^2-1}e^{2\hat{\gamma}}\,, \end{aligned} \tag{8.0.2}$$

where

$$\begin{aligned} R &= a_+a_- + b_+b_-\,, \qquad L = a_+^2 + b_+^2\,, \\ \mathfrak{M} &= \alpha x(1-y^2)(e^{2q\delta_+} + e^{2q\delta_-})a_+ + y(x^2-1)(1-\alpha^2 e^{2q(\delta_+ + \delta_-)})b_+\,, \\ \hat{\gamma} &= \frac{1}{2}(1+q)^2\ln\frac{x^2-1}{x^2-y^2} + 2q(1-P_2)Q_1 + q^2(1-P_2)\Big[(1+P_2)(Q_1^2-Q_2^2) \\ &\quad + \frac{1}{2}(x^2-1)(2Q_2^2 - 3xQ_1Q_2 + 3Q_0Q_2 - Q_2')\Big]\,. \end{aligned} \tag{8.0.3}$$

Here $P_l(y)$ and $Q_l(x)$ are Legendre polynomials of the first and second kind respectively. Furthermore

$$\begin{aligned} a_\pm &= x(1-\alpha^2 e^{2q(\delta_+ + \delta_-)}) \pm (1+\alpha^2 e^{2q(\delta_+ + \delta_-)})\,, \\ b_\pm &= \alpha y(e^{2q\delta_+} + e^{2q\delta_-}) \mp \alpha(e^{2q\delta_+} - e^{2q\delta_-})\,, \\ \delta_\pm &= \frac{1}{2}\ln\frac{(x\pm y)^2}{x^2-1} + \frac{3}{2}(1-y^2\mp xy) + \frac{3}{4}[x(1-y^2)\mp y(x^2-1)]\ln\frac{x-1}{x+1}\,, \end{aligned} \tag{8.0.4}$$

the quantity α being a constant

$$\alpha = \frac{\sigma - M}{a}\,, \qquad \sigma = \sqrt{M^2 - a^2}\,. \tag{8.0.5}$$

The Geroch-Hansen moments are given by

$$M_{2k+1} = J_{2k} = 0\,, \quad k = 0,1,2,... \tag{8.0.6}$$

$$M_0 = M\,, \quad M_2 = -Ma^2 + \frac{2}{15}qM^3\left(1-\frac{a^2}{M^2}\right)^{3/2}\,,... \tag{8.0.7}$$

$$J_1 = Ma\,, \quad J_3 = -Ma^3 + \frac{4}{15}qM^3a\left(1-\frac{a^2}{M^2}\right)^{3/2}\,,.... \tag{8.0.8}$$

The vanishing of the odd gravitoelectric (M_n) and even gravitomagnetic (J_n) multipole moments is a consequence of the reflection symmetry of the so-

lution about the hyperplane $y = 0$, which we will refer to as "symmetry" (or equivalently "equatorial") plane hereafter. From the above expressions we see that M is the total mass of the body, a represents the specific angular momentum, and q is related to the deviation from spherical symmetry. All higher multipole moments can be shown to depend only on the parameters M, a, and q.

We limit our analysis here to the case $\sigma > 0$, i.e. $M > a$. In the case $\sigma = 0$ the solution reduces to the extreme Kerr spacetime irrespective of the value of q. The case σ complex, i.e. $a > M$, requires a different definition of the quadrupole parameter in order to have real Geroch-Hansen moments and can be better discussed by using Weyl cylindrical coordinates. We will not explore this case here.

In this work we analyze some geometric and physical properties of the QM solution. The limiting cases contained in the general solution suggest that it can be used to describe the exterior asymptotically flat gravitational field of a rotating body with arbitrary quadrupole moment. This is confirmed by the analysis of the motion of particles on the equatorial plane. It turns out that the whole geometric structure of the QM spacetime is drastically changed in comparison with Kerr spacetime, leading to a number of previously unexplored physical effects strongly modifying the features of particle motion, especially near the gravitational source. In fact, the QM solution is characterized by a naked singularity at $x = 1$, whose existence critically depends on the value of the quadrupole parameter q. In the case $q = 0$ (Kerr solution) $x = 1$ represents instead an event horizon. This bifurcating behaviour accounts for the above mentioned drastic changes with respect to the Kerr metric.

Due to the very complicated form of the metric most of the analysis will be performed numerically.

8.1 Limiting cases

The QM solution reduces to the Kerr spacetime in the limiting case $q \to 0$ and to the Erez-Rosen spacetime when $a \to 0$. Furthermore, it can be shown that the general form of the QM solution (see Appendix A) is equivalent, up to a coordinate transformation, to the exterior vacuum Hartle-Thorne solution once linearized to first order in the quadrupole parameter and to second order in the rotation parameter.

8.1.1 Kerr solution

For vanishing quadrupole parameter we recover the Kerr solution, with functions

$$\begin{aligned} f_K &= \frac{c^2x^2+d^2y^2-1}{(cx+1)^2+d^2y^2}\,, \quad \omega_K = 2a\frac{(cx+1)(1-y^2)}{c^2x^2+d^2y^2-1}\,, \\ \gamma_K &= \frac{1}{2}\ln\left(\frac{c^2x^2+d^2y^2-1}{c^2(x^2-y^2)}\right)\,, \end{aligned} \tag{8.1.1}$$

where

$$c=\frac{\sigma}{M}\,, \quad d=\frac{a}{M}\,, \quad c^2+d^2=1\,, \tag{8.1.2}$$

so that $\alpha = (c-1)/d$. Transition of this form of Kerr metric to the more familiar one associated with Boyer-Lindquist coordinates is accomplished by the map

$$x=\frac{r-M}{\sigma}\,, \qquad y=\cos\theta\,, \tag{8.1.3}$$

so that $x=1$ corresponds to the outer horizon $r=r_+=M+\sigma$.

To first order in q the QM solution becomes

$$\begin{aligned} f &= f_K - 2q[P_2Q_2f_K + \Lambda_+\delta_+ + \Lambda_-\delta_-] + O(q^2)\,, \\ \omega &= \omega_K + 2acq\left[2P_2Q_2\frac{c(x^2-y^2)+x(1-y^2)}{c^2x^2+d^2y^2-1} + \Psi_+\delta_+ + \Psi_-\delta_-\right] + O(q^2)\,, \\ \gamma &= \gamma_K + q\left[2(1-P_2)Q_1 + \ln\left(\frac{x^2-1}{x^2-y^2}\right)\right. \\ &\quad \left. +\alpha d\frac{c(x^2-y^2)+1-y^2}{c^2x^2+d^2y^2-1}(\delta_+ + \delta_-)\right] + O(q^2)\,, \end{aligned} \tag{8.1.4}$$

where

$$\begin{aligned} \Lambda_\pm &= d^2(x\pm y)\frac{[c(x\mp y)+1]^2-y^2}{[(cx+1)^2+d^2y^2]^2}\,, \\ \Psi_\pm &= \frac{x\pm y}{(c^2x^2+d^2y^2-1)^2}\{cd^2(x\mp y)^2(1\pm xy) + c(x^2-1)(1\mp xy) \\ &\quad +(x\mp y)[c^2(x^2-1)+d^2(1-y^2)]\}\,. \end{aligned} \tag{8.1.5}$$

This approximate metric could be used to describe the exterior field of an arbitrarily rotating mass source with a small quadrupole moment. The lowest Geroch-Hansen multipole moments in this case coincide with those of the exact solution as given in Eqs. (8.0.7) and (8.0.8). Differences will appear in higher moments where all terms containing q^2 and higher exponents must be neglected.

It is interesting to mention that in the limiting case $a \to M$, the QM metric

leads to the extreme Kerr black hole solution, regardless of the value of the quadrupole q. This can be easily seen both at the level of the multipole moments (8.0.7) and (8.0.8) and by directly computing the limiting metric. The latter determines in turn the limit of applicability of the QM solution, since for values in the range $a/M > 1$ the multipole moments and the metric both become complex. As stated in the Introduction we will not consider such a situation here.

8.1.2 Erez-Rosen solution

Similarly, for vanishing rotation parameter we recover the Erez-Rosen solution. It is a solution of the static Weyl class of solutions (i.e. $\omega = 0$) with functions

$$f_{ER} = \frac{x-1}{x+1} e^{-2qP_2Q_2}\,, \qquad \gamma_{ER} = \hat{\gamma}\,, \tag{8.1.6}$$

which reduce to

$$f_S = \frac{x-1}{x+1}\,, \qquad \gamma_S = \frac{1}{2}\ln\left(\frac{x^2-1}{x^2-y^2}\right) \tag{8.1.7}$$

when $q = 0$, corresponding to the Schwarzschild solution.

To first nonvanishing order in a/M we find

$$\begin{aligned}
f &= f_{ER}\left\{1 + \frac{1}{2(x^2-1)(x+1)}\left[(x+y)(y-1)e^{4q\delta_+} - (x-y)(y+1)e^{4q\delta_-}\right.\right. \\
&\quad \left.\left. -2(x^2-y^2)e^{2q(\delta_+ + \delta_-)}\right]\left(\frac{a}{M}\right)^2\right\} + O[(a/M)^4]\,, \\
\omega &= -2M\left\{1 + \frac{e^{2qP_2Q_2}}{2(x-1)}\left[(x+y)(y-1)e^{2q\delta_+} - (x-y)(y+1)e^{2q\delta_-}\right]\right\}\frac{a}{M} \\
&\quad + O[(a/M)^3]\,, \\
\gamma &= \gamma_{ER} + \frac{1}{4}\left\{1 - \frac{1}{2(x^2-1)}\left[(1-y^2)(e^{4q\delta_+} + e^{4q\delta_-})\right.\right. \\
&\quad \left.\left. +2(x^2-y^2)e^{2q(\delta_+ + \delta_-)}\right]\right\}\left(\frac{a}{M}\right)^2 + O[(a/M)^4]\,.
\end{aligned} \tag{8.1.8}$$

This approximate solution can be interpreted as a generalization of the Lense-Thirring spacetime, which is obtained in the limit $q \to 0$ by retaining terms up to the linear order in a/M. Consequently, the approximate solution (8.1.8) could be used to investigate the exterior gravitational field of slowly rotating deformed bodies. A similar approximate solution, accurate to second order in the rotation parameter and to first order in the quadrupole moment, was found long ago by Hartle and Thorne.

8.1.3 Hartle-Thorne solution

The Hartle-Thorne metric describing the exterior field of a slowly rotating slightly deformed object is given by

$$\begin{aligned} \mathrm{d}s^2 &= -\left(1-\frac{2\mathcal{M}}{R}\right)\left[1+2k_1P_2(\cos\Theta)+2\left(1-\frac{2\mathcal{M}}{R}\right)^{-1}\frac{\mathcal{J}^2}{R^4}(2\cos^2\Theta-1)\right]\mathrm{d}t^2 \\ &\quad +\left(1-\frac{2\mathcal{M}}{R}\right)^{-1}\left[1-2k_2P_2(\cos\Theta)-2\left(1-\frac{2\mathcal{M}}{R}\right)^{-1}\frac{\mathcal{J}^2}{R^4}\right]\mathrm{d}R^2 \\ &\quad +R^2(\mathrm{d}\Theta^2+\sin^2\Theta\mathrm{d}\phi^2)[1-2k_3P_2(\cos\Theta)]-4\frac{\mathcal{J}}{R}\sin^2\Theta\mathrm{d}t\mathrm{d}\phi\,, \end{aligned} \tag{8.1.9}$$

where

$$\begin{aligned} k_1 &= \frac{\mathcal{J}^2}{\mathcal{M}R^3}\left(1+\frac{\mathcal{M}}{R}\right)-\frac{5}{8}\frac{\mathcal{Q}-\mathcal{J}^2/\mathcal{M}}{\mathcal{M}^3}Q_2^2\left(\frac{R}{\mathcal{M}}-1\right)\,, \\ k_2 &= k_1-\frac{6\mathcal{J}^2}{R^4}\,, \\ k_3 &= k_1+\frac{\mathcal{J}^2}{R^4}-\frac{5}{4}\frac{\mathcal{Q}-\mathcal{J}^2/\mathcal{M}}{\mathcal{M}^2R}\left(1-\frac{2\mathcal{M}}{R}\right)^{-1/2}Q_2^1\left(\frac{R}{\mathcal{M}}-1\right)\,. \end{aligned} \tag{8.1.10}$$

Here Q_l^m are the associated Legendre functions of the second kind and the constants $\mathcal{M}$, $\mathcal{J}$ and $\mathcal{Q}$ are the total mass, angular momentum and mass quadrupole moment of the rotating star respectively.

It is interesting to find out the connection between the Hartle-Thorne solution and the QM solution in the appropriate limit. To this end it is necessary to start with the general form of the QM solution as given in Appendix A containing an additional parameter, the Zipoy-Voorhees constant parameter δ. For our purposes it is convenient to set such a parameter as $\delta = 1+sq$, where s is a real number. For $s=0$, i.e. $\delta=1$, we recover the solution (8.0.1)–(8.0.5). To first order in the quadrupole parameter q and to second order in the rotation parameter a/M the metric functions turn out to be

$$\begin{aligned} f &\simeq \frac{x-1}{x+1}\left[1-q\left(2P_2Q_2-s\ln\frac{x-1}{x+1}\right)\right]-\frac{x^2+x-2y^2}{(x+1)^3}\left(\frac{a}{M}\right)^2\,, \\ \omega &\simeq 2M\frac{1-y^2}{x-1}\left(\frac{a}{M}\right)\,, \\ \gamma &\simeq \hat{\gamma}(1+2sq)-\frac{1}{2}\frac{1-y^2}{x^2-1}\left(\frac{a}{M}\right)^2\,, \end{aligned} \tag{8.1.11}$$

where $\hat{\gamma}$ is defined in Eq. (8.0.3) and terms of the order of $q(a/M)$ have also been neglected.

Introduce first Boyer-Lindquist coordinates (t,r,θ,ϕ) through the transfor-

mation

$$t = t\,, \qquad x = \frac{r-M}{\sigma}\,, \qquad y = \cos\theta\,, \qquad \phi = \phi\,. \tag{8.1.12}$$

Then set $s = -1$ and $M = M'(1+q)$. The further transformation

$$t = t\,, \qquad r = r(R,\Theta)\,, \qquad \theta = \theta(R,\Theta)\,, \qquad \phi = \phi \tag{8.1.13}$$

with

$$\begin{aligned} r &= R + M'q + \frac{3}{2}M'q\sin^2\Theta\left[\frac{R}{M'} - 1 + \frac{1}{2}\frac{R^2}{M'^2}\left(1-\frac{2M'}{R}\right)\ln\left(1-\frac{2M'}{R}\right)\right] \\ &\quad -\frac{a^2}{2R}\left[\left(1+\frac{2M'}{R}\right)\left(1-\frac{M'}{R}\right) - \cos^2\Theta\left(1-\frac{2M'}{R}\right)\left(1+\frac{3M'}{R}\right)\right]\,, \\ \theta &= \Theta - \sin\Theta\cos\Theta\left\{\frac{3}{2}q\left[2+\left(\frac{R}{M'}-1\right)\ln\left(1-\frac{2M'}{R}\right)\right] + \frac{a^2}{2R^2}\left(1+\frac{2M'}{R}\right)\right\} \end{aligned} \tag{8.1.14}$$

finally gives the mapping between the general form of QM solution and the Hartle-Thorne metric (8.1.9) with parameters

$$\mathcal{M} = M' = M(1-q)\,, \quad \mathcal{J} = -Ma\,, \quad \mathcal{Q} = \frac{\mathcal{J}^2}{M} + \frac{4}{5}M^3 q\,. \tag{8.1.15}$$

Note that the previous transformation is obtained simply by combining the corresponding transformation from Kerr to Hartle-Thorne solution as given by Hartle and Thorne themselves and that from Erez-Rosen to Hartle-Thorne solution as found by Mashhoon and Theiss.

8.2 Geometric properties of the solution

The solution admits two Killing vectors associated with translation in time and rotation about the symmetry axis. The timelike Killing vector ∂_t changes its causality property when $f = 0$, defining a hypersurface which in the Kerr limiting case is called ergosurface as the boundary of the ergosphere (or equivalently ergoregion). Using this terminology also in this case we compare in Figs. 8.1 and 8.2 the ergoregions of Kerr solution and QM solution (for different values of the quadrupole parameter) respectively. The situation is completely different. In fact, while in the Kerr case such a hypersurface is the boundary of a simply-connected domain, in the case of the QM solution this property is no more true, as soon as the magnitude of the quadrupole parameter exceeds a certain critical value (for example, for the choice $a/M = 0.5$ the range of Kerr-like behaviour corresponds to $-1 \lesssim q \lesssim 1.21$).

The spacelike Killing vector ∂_ϕ also changes its causality condition in some regions, leading to the existence of closed timelike curves in the QM solution. These regions are depicted in Fig. 8.3 for different values of the quadrupole parameter.

In order to investigate the structure of singularities in the QM metric we have to consider the curvature invariants. Since the solution is a vacuum one there exist just two independent quadratic scalar invariants, the Kretschmann invariant K_1 and the Chern-Pontryagin invariant K_2 defined by

$$K_1 = R^{\alpha\beta\gamma\delta} R_{\alpha\beta\gamma\delta} \,, \qquad K_2 = {}^*R^{\alpha\beta\gamma\delta} R_{\alpha\beta\gamma\delta} \,, \tag{8.2.1}$$

where the star denotes the dual. The behaviour of curvature invariants as functions of x for selected values of y, a/M and q is shown in Fig. 8.4. It turns out that K_1 diverges when approaching $x = 1$ along the direction $y = 0$, but it is finite there moving along a different path. Furthermore, the invariant K_2 vanishes identically for $y = 0$. Therefore, the metric has a directional singularity at $x = 1$.

It is now interesting to investigate what kind of hypersurface is $x = 1$. Consider the normal to a $x =$ const hypersurface. The behaviour of its norm g^{xx} when approaching $x = 1$ discriminates between its character being either null or timelike depending on the value of the quadrupole parameter. The limit of g^{xx} as $x \to 1$ also depends on y. For instance, approaching $x = 1$ along any direction on the equatorial plane $y = 0$ gives

$$g^{xx} \sim (x-1)^{1+q/2-q^2/4} \,, \tag{8.2.2}$$

implying that the singular hypersurface $x = 1$ is null when $|q - 1| < \sqrt{5}$ and timelike otherwise. On the other hand, moving along the axis $y = 1$ gives

$$g^{xx} \sim \begin{cases} (x-1)^{1+q} \,, & q > 0 \\ (x-1) \,, & -1 < q < 0 \\ (x-1)^{-q} \,, & q < -1 \,, \end{cases} \tag{8.2.3}$$

implying that the singular hypersurface $x = 1$ is always null.

A similar discussion can be done also for the metric determinant. Approaching $x = 1$ along any direction on the equatorial plane $y = 0$ gives

$$\sqrt{-g} \sim (x-1)^{-q/2+q^2/4} \,, \tag{8.2.4}$$

implying that the volume element vanishes approaching the singular hypersurface $x = 1$ when $q < 0$, $q > 2$ and diverges otherwise. On the other hand,

moving along the axis $y = 1$ gives

$$\sqrt{-g} \sim \begin{cases} (x-1)^{-q}\,, & q > 0 \\ \text{const}\,, & -1 < q < 0 \\ (x-1)^{q+1}\,, & q < -1\,. \end{cases} \tag{8.2.5}$$

We note that if the presence of the quadrupole moment totally changes the situation with respect to the Kerr spacetime, the smooth horizon of the Kerr solution becoming a singular hypersurface in the QM solution, the properties of the naked singularity are also different with respect to the limiting case of the Erez-Rosen spacetime.

Finally, the spectral index S (see Appendix B for the definition of S in terms of Weyl scalars) shows that the solution is algebraically general. The real part of S is plotted in Fig. 8.5 as a function of x for $y = 0$ and selected values of a/M and q. The imaginary part is identically zero in this case. A numerical analysis of the spectral index for different values of the quadrupole moment shows that $S \to 1$ as $x \to \infty$, i.e. it is algebraically special. We conclude that the asymptotic behavior of the spacetime is dominated by the Kerr spacetime which is algebraically special of type D. This is in agreement with the expectation which follows from the analysis of relativistic multipole moments, according to which any stationary axisymmetric asymptotically flat vacuum solution of Einstein's equations must approach the Kerr metric asymptotically.

Note that drawing a Penrose diagram would help to easier understand the global aspects of the geometry of the QM solution. However, due to the rather involved form of the metric functions it is a very hard task to construct it. Analytic calculations can be performed only in the case of small values of the quadrupole parameter q. But in this simplest case ($q \ll 1$) it is possible to show that the resulting conformal diagram is closely similar to the corresponding one for a Kerr naked singularity.

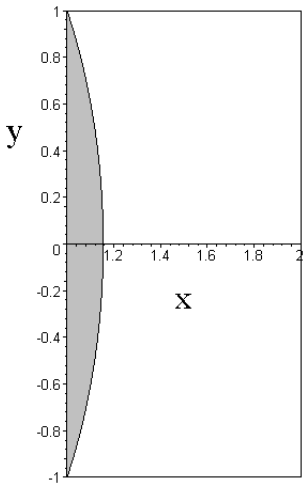

Figure 8.1: The shape of the ergoregion is shown in the case of vanishing quadrupole parameter $q = 0$ (Kerr spacetime) for the choice $a/M = 0.5$ in prolate spheroidal coordinates.

8.3 Geodesics

The geodesic motion of test particles is governed by the following equations:

$$\begin{aligned}
\dot{t} &= \frac{E}{f} + \frac{\omega f}{\sigma^2 X^2 Y^2}(L - \omega E)\,, \qquad \dot{\phi} = \frac{f}{\sigma^2 X^2 Y^2}(L - \omega E)\,, \\
\ddot{y} &= -\frac{1}{2}\frac{Y^2}{X^2}\left[\frac{f_y}{f} - 2\gamma_y + \frac{2y}{X^2+Y^2}\right]\dot{x}^2 + \left[\frac{f_x}{f} - 2\gamma_x - \frac{2x}{X^2+Y^2}\right]\dot{x}\dot{y} \\
&\quad + \frac{1}{2}\left[\frac{f_y}{f} - 2\gamma_y - \frac{2y}{X^2+Y^2}\frac{X^2}{Y^2}\right]\dot{y}^2 - \frac{1}{2}\frac{e^{-2\gamma}}{f\sigma^4 X^2 Y^2 (X^2+Y^2)}\Big\{Y^2[f^2(L-\omega E)^2 \\
&\quad + E^2\sigma^2 X^2 Y^2]f_y + 2(L-\omega E)f^3[y(L-\omega E) - EY^2\omega_y]\Big\}\,, \\
\dot{x}^2 &= -\frac{X^2}{Y^2}\dot{y}^2 + \frac{e^{-2\gamma}X^2}{\sigma^2(X^2+Y^2)}\left[E^2 - \mu^2 f - \frac{f^2}{\sigma^2 X^2 Y^2}(L-\omega E)^2\right]\,,
\end{aligned} \tag{8.3.1}$$

where Killing symmetries and the normalization condition have been used. Here E and L are the energy and angular momentum of the test particle respectively, μ is the particle mass and dot denotes differentiation with respect to the affine parameter; furthermore, the notation

$$X = \sqrt{x^2 - 1}\,, \quad Y = \sqrt{1 - y^2} \tag{8.3.2}$$

has been introduced.

Let us consider the motion on the symmetry plane $y = 0$. If $y = 0$ and

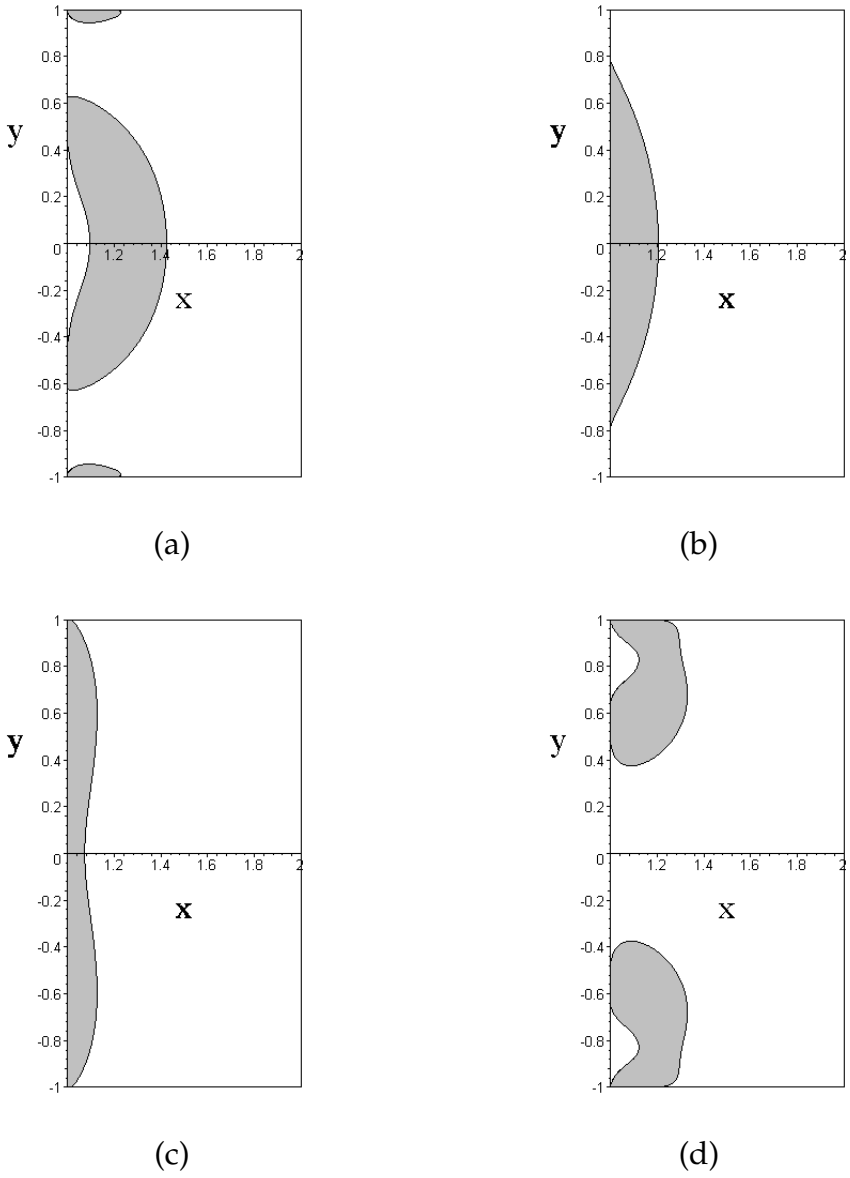

Figure 8.2: The shape of the ergoregion is shown for $a/M = 0.5$ and different values of the quadrupole parameter: $q = [-10, -1, 1, 10]$, from (a) to (d) respectively. For $q = -1$ and $q = 1$ the shape is similar to the Kerr case, i.e. the regions are simply-connected.

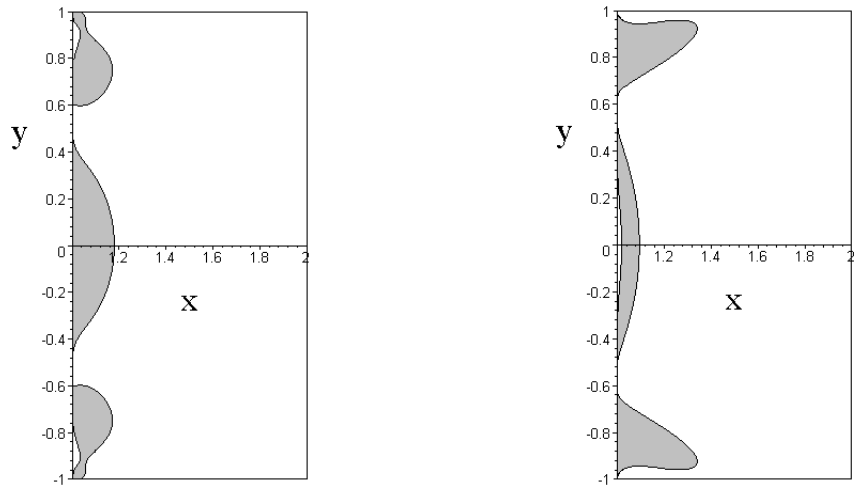

(a) (b)

Figure 8.3: The regions where the metric component $g_{\phi\phi}$ changes its sign are shown for $a/M = 0.5$ and different values of the quadrupole parameter: (a) $q = 10$ and (b) $q = -10$. The existence of closed timelike curves is allowed there.

$\dot{y} = 0$ initially, Eq. $(8.3.1)_3$ ensures that the motion will be confined on the symmetry plane, since f_y, ω_y and γ_y all vanish at $y = 0$, so that $\ddot{y} = 0$ too. Eqs. (8.3.1) thus reduce to

$$\begin{aligned} \dot{t} &= \frac{E}{f} + \frac{\omega f}{\sigma^2 X^2}(L - \omega E) \,, \qquad \dot{\phi} = \frac{f}{\sigma^2 X^2}(L - \omega E) \,, \\ \dot{x}^2 &= \frac{e^{-2\gamma} X^2}{\sigma^2 (1 + X^2)} \left[E^2 - \mu^2 f - \frac{f^2}{\sigma^2 X^2}(L - \omega E)^2 \right] \,, \end{aligned} \tag{8.3.3}$$

where metric functions are meant to be evaluated at $y = 0$. The motion turns out to be governed by the effective potential V defined by the equation

$$V^2 - \mu^2 f - \frac{f^2}{\sigma^2 X^2}(L - \omega V)^2 = 0 \,. \tag{8.3.4}$$

In fact, for $E = V$ the rhs of Eq. $(8.3.3)_3$ vanishes.

The behaviour of V as a function of x is shown in Fig. 8.6. Repulsive effects occur for decreasing values of x approaching $x = 1$.

The case of a geodesic particle at rest will be analyzed below. Circular geodesics will be discussed in detail in the next section, where accelerated orbits are also studied.

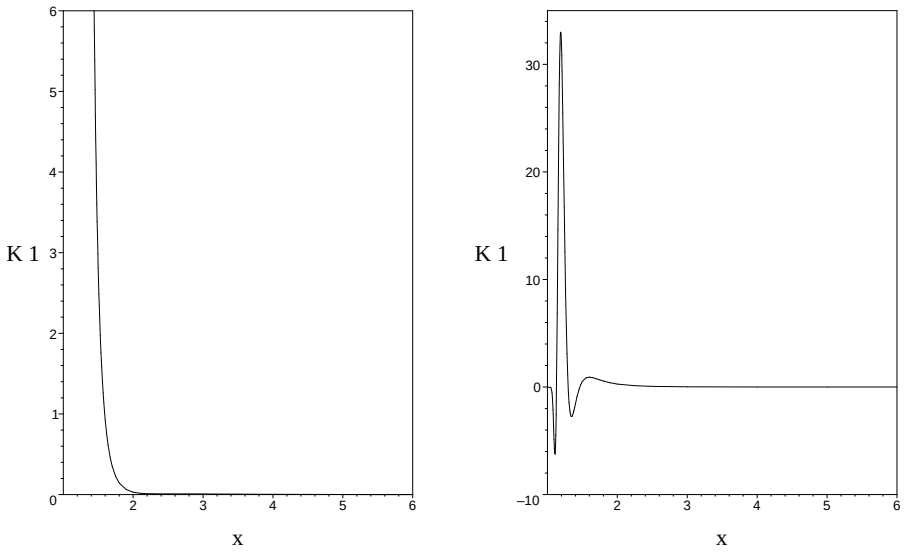

(a) (b)

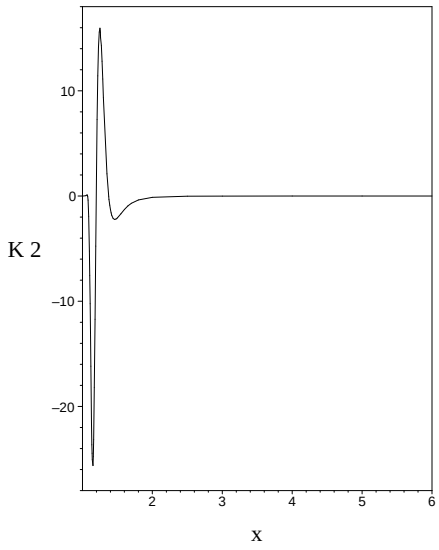

(c)

Figure 8.4: The behaviour of the Kretschmann invariant K_1 as a function of x is shown for the choice of parameters $a/M = 0.5$ and $q = 10$ for different values of y: (a) $y = 0$ and (b) $y = 0.5$. Figure (c) shows instead the behaviour of the Chern-Pontryagin invariant K_2 for the same choice of parameters as in Fig. (b). Figs. (b) and (c) show how both the invariants K_1 and K_2 change their signs as x approaches unity. This is a manifestation of the appearence of repulsive gravity regions, typical of naked singularity solutions. When $x \to \infty$ the invariants K_1 and K_2 both vanish, as expected.

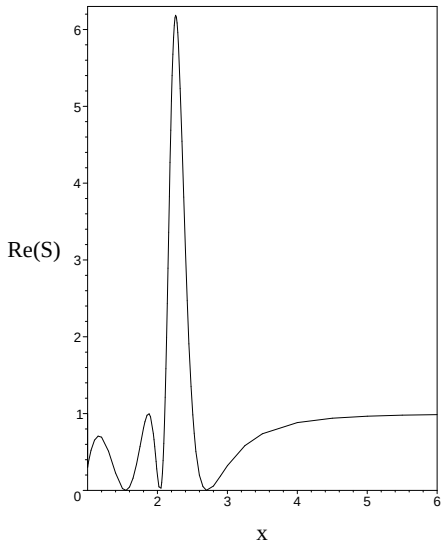

Figure 8.5: The behaviour of the real part of the speciality index S as a function of x is shown for the choice of parameters $a/M = 0.5$, $q = 10$ and $y = 0$. In this case ($y = 0$) we have also $\mathrm{Im}(S) \equiv 0$.

8.3.1 Particle at rest

For the QM solution which is characterized by the presence of a naked singularity it is even possible to satisfy the conditions for a geodesic particle to be at rest for certain values of the quadrupole moment. This effect can be explained when the attractive behaviour of gravity is balanced by a repulsive force exerted by the naked singularity. Usually, repulsive effects are interpreted as a consequence of the presence of an effective mass which varies with distance and can thus become negative. The consideration of the corresponding post-Newtonian limit shows that an effective mass can be indeed introduced, depending on the distance from the source and the value of the Geroch-Hansen quadrupole moment. We see that in the case of the corresponding exact solution under consideration a similar situation takes place.

A particle at rest is characterized by the four velocity

$$U = \frac{1}{\sqrt{f}}\partial_t \,. \tag{8.3.5}$$

The corresponding four acceleration $a(U) = \nabla_U U$ is given by

$$a(U) = \frac{e^{-2\gamma}}{2\sigma^2(X^2+Y^2)}[X^2 f_x \partial_x + Y^2 f_y \partial_y] \,. \tag{8.3.6}$$

On the symmetry plane $y = 0$ we have $f_y = 0$, so that the geodesic condition $a(U) = 0$ implies $f_x = 0$. The pairs (x, q) satisfying this condition are shown

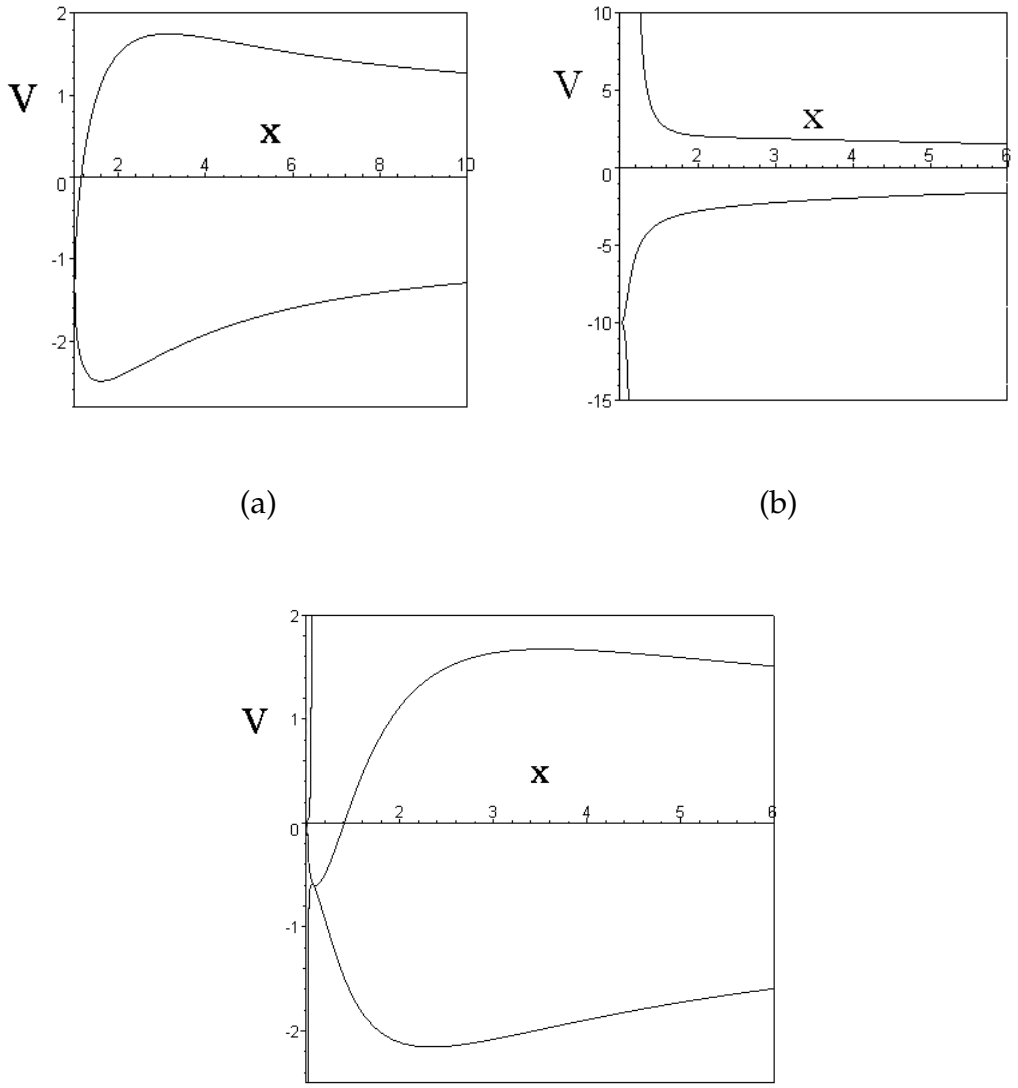

(a) (b)

(c)

Figure 8.6: The behaviour of the effective potential V as a function of x is shown for the choice of parameters $a/M = 0.5$ and $L/(\mu M) = 10$ for different values of the quadrupole parameter: (a) $q = 0$, (b) $q = 10$ and (c) $q = -10$.

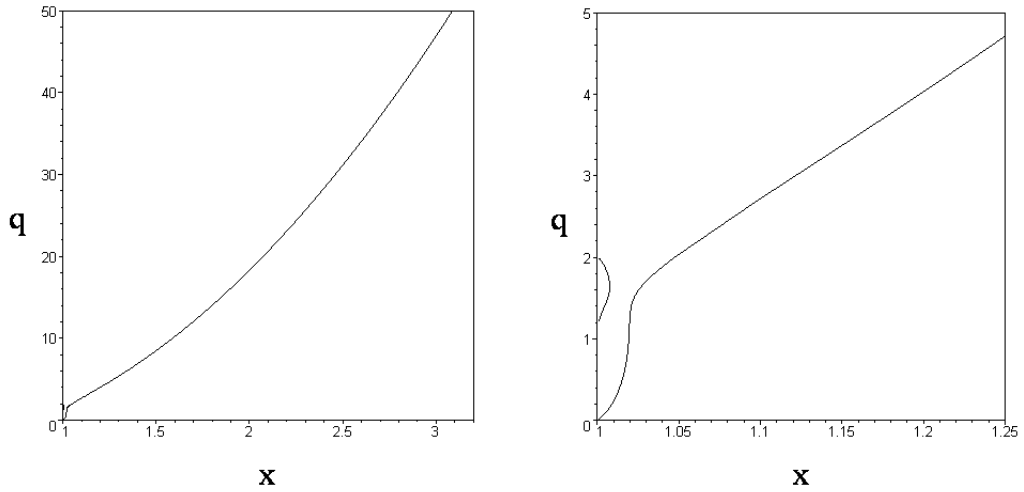

(a) (b)

Figure 8.7: The pairs (x, q) allowing a test particle to be at rest in the QM spacetime are shown for $a/M = 0.5$. Fig. (b) is a detail of Fig. (a) close to $x = 1$. No equilibrium positions exist for $q \leq 0$.

in Fig. 8.7 for a fixed value of a/M. As an example, for $a/M = 0.5$ and $q = 10$ we get $x \approx 1.588$ as the equilibrium position. In this case the corresponding energy and angular momentum per unit mass of the particle are given by $E/\mu \approx 0.553$ and $L/(\mu M) \approx 0.257$ respectively. No equilibrium positions exist for $q \leq 0$.

8.4 Circular orbits on the symmetry plane

Let us introduce the ZAMO family of fiducial observers, with four velocity

$$n = N^{-1}(\partial_t - N^\phi \partial_\phi); \tag{8.4.1}$$

here $N = (-g^{tt})^{-1/2}$ and $N^\phi = g_{t\phi}/g_{\phi\phi}$ are the lapse and shift functions respectively. A suitable orthonormal frame adapted to ZAMOs is given by

$$e_{\hat{t}} = n, \quad e_{\hat{x}} = \frac{1}{\sqrt{g_{xx}}}\partial_x, \quad e_{\hat{y}} = \frac{1}{\sqrt{g_{yy}}}\partial_y, \quad e_{\hat{\phi}} = \frac{1}{\sqrt{g_{\phi\phi}}}\partial_\phi, \tag{8.4.2}$$

with dual

$$\omega^{\hat{t}} = N\mathrm{d}t\,, \quad \omega^{\hat{x}} = \sqrt{g_{xx}}\mathrm{d}x\,, \quad \omega^{\hat{y}} = \sqrt{g_{yy}}\mathrm{d}y\,, \quad \omega^{\hat{\phi}} = \sqrt{g_{\phi\phi}}(\mathrm{d}\phi + N^\phi \mathrm{d}t)\,. \tag{8.4.3}$$

The 4-velocity U of uniformly rotating circular orbits can be parametrized

either by the (constant) angular velocity with respect to infinity ζ or, equivalently, by the (constant) linear velocity v with respect to ZAMOs

$$U = \Gamma[\partial_t + \zeta\partial_\phi] = \gamma[e_{\hat{t}} + v e_{\hat{\phi}}], \qquad \gamma = (1 - v^2)^{-1/2}\,, \tag{8.4.4}$$

where Γ is a normalization factor which assures that $U_\alpha U^\alpha = -1$ given by:

$$\Gamma = \left[N^2 - g_{\phi\phi}(\zeta + N^\phi)^2\right]^{-1/2} = \frac{\gamma}{N} \tag{8.4.5}$$

and

$$\zeta = -N^\phi + \frac{N}{\sqrt{g_{\phi\phi}}}v. \tag{8.4.6}$$

We limit our analysis to the motion on the symmetry plane ($y = 0$) of the solution (8.0.1)–(8.0.5). Note both $y = 0$ and $x = x_0$ are constants along any given circular orbit, and that the azimuthal coordinate along the orbit depends on the coordinate time t or proper time τ along that orbit according to

$$\phi - \phi_0 = \zeta t = \Omega_U \tau_U\,, \quad \Omega_U = \Gamma\zeta\,, \tag{8.4.7}$$

defining the corresponding coordinate and proper time orbital angular velocities ζ and Ω_U. These determine the rotation of the spherical frame with respect to a nonrotating frame at infinity.

The spacetime Frenet-Serret frame along a single timelike test particle worldline with 4-velocity $U = E_0$ and parametrized by the proper time τ_U is described by the following system of evolution equations

$$\begin{aligned} \frac{DE_0}{d\tau_U} &= \kappa E_1\,, & \frac{DE_1}{d\tau_U} &= \kappa E_0 + \tau_1 E_2\,, \\ \frac{DE_2}{d\tau_U} &= -\tau_1 E_1 + \tau_2 E_3\,, & \frac{DE_3}{d\tau_U} &= -\tau_2 E_2\,. \end{aligned} \tag{8.4.8}$$

The absolute value of the curvature κ is the magnitude of the acceleration $a(U) \equiv DU/d\tau_U = \kappa E_1$, while the first and second torsions τ_1 and τ_2 are the components of the Frenet-Serret angular velocity vector

$$\omega_{(\mathrm{FS})} = \tau_1 E_3 + \tau_2 E_1\,, \qquad ||\omega_{(\mathrm{FS})}|| = [\tau_1^2 + \tau_2^2]^{1/2}\,, \tag{8.4.9}$$

with which the spatial Frenet-Serret frame $\{E_a\}$ rotates with respect to a Fermi-Walker transported frame along U. It is well known that any circular orbit on the symmetry plane of a reflection symmetric spacetime has zero second torsion τ_2, while the geodesic curvature κ and the first torsion τ_1 are simply related by

$$\tau_1 = -\frac{1}{2\gamma^2}\frac{\mathrm{d}\kappa}{\mathrm{d}v}\,. \tag{8.4.10}$$

On the symmetry plane there exists a large variety of special circular orbits; particular interest is devoted to the co-rotating $(+)$ and counter-rotating $(-)$ timelike circular geodesics whose linear velocities is

$$\nu_{(\mathrm{geo})\pm} \equiv \nu_{\pm} = \frac{fC \pm \left[f^2\omega^2 - \sigma^2(x^2-1)\right]\sqrt{D}}{\sqrt{x^2-1}\sigma\{f_x[f^2\omega^2 + \sigma^2(x^2-1)] + 2f(f^2\omega\omega_x - \sigma^2 x)\}} , \tag{8.4.11}$$

where

$$\begin{aligned} C &= -2\sigma^2(x^2-1)\omega f_x - f\{\omega_x[f^2\omega^2 + \sigma^2(x^2-1)] - 2\sigma^2 x\omega\} , \\ D &= f^4\omega_x^2 - \sigma^2 f_x[f_x(x^2-1) - 2xf] . \end{aligned} \tag{8.4.12}$$

All quantities in the previous expressions are meant to be evaluated at $y = 0$. The corresponding timelike conditions $|\nu_{\pm}| < 1$ together with the reality condition $D \geq 0$ identify the allowed regions for the "radial" coordinate where co/counter-rotating geodesics exist.

Other special orbits correspond to the "geodesic meeting point observers" with

$$\nu_{(\mathrm{gmp})} = \frac{\nu_+ + \nu_-}{2} . \tag{8.4.13}$$

A Frenet-Serret (FS) intrinsic frame along U is given by

$$E_0 \equiv U = \gamma[n + \nu e_{\hat{\phi}}] , \quad E_1 = e_{\hat{x}} , \quad E_2 = e_{\hat{y}} , \quad E_2 \equiv E_{\hat{\phi}} = \gamma[\nu n + e_{\hat{\phi}}] . \tag{8.4.14}$$

It is also convenient to introduce the Lie relative curvature of each orbit

$$\begin{aligned} k_{(\mathrm{lie})} &= -\partial_{\hat{x}} \ln\sqrt{g_{\phi\phi}} \\ &= \frac{e^{-\gamma}\sqrt{x^2-1}}{2\sigma x\sqrt{f}} \left\{ \frac{\sigma^2[(x^2-1)f_x - 2xf] + f^2\omega(2f\omega_x + \omega f_x)}{\sigma^2(x^2-1) - f^2\omega^2} \right\} . \end{aligned} \tag{8.4.15}$$

It then results

$$\begin{aligned} \kappa &= k_{(\mathrm{lie})}\gamma^2(\nu - \nu_+)(\nu - \nu_-) , \\ \tau_1 &= k_{(\mathrm{lie})}\nu_{(\mathrm{gmp})}\gamma^2(\nu - \nu_{(\mathrm{crit})+})(\nu - \nu_{(\mathrm{crit})-}) , \end{aligned} \tag{8.4.16}$$

where

$$\nu_{(\mathrm{crit})\pm} = \frac{\gamma_-\nu_- \mp \gamma_+\nu_+}{\gamma_- \mp \gamma_+} , \qquad \nu_{(\mathrm{crit})+}\nu_{(\mathrm{crit})-} = 1 , \tag{8.4.17}$$

identify the so called "extremely accelerated observers": $\nu_{(\mathrm{ext})} \equiv \nu_{(\mathrm{crit})-}$, which satisfies the timelike condition in the regions where timelike geodesics

exist, while $v_{(\mathrm{crit})+}$ is always spacelike there.

The geodesic velocities (8.4.11) are plotted in Fig. 8.8 both as functions of the quadrupole parameter q for fixed "radial" distance (see Fig. (a)) and as functions of x for different values of q (see Fig. (b)). In the first case (Fig. (a)) we have shown how the quadrupole moment affects the causality condition: there exist a finite range of values of q wherein timelike circular geodesics are allowed: $q_1 < q < q_3$ for co-rotating and $q_2 < q < q_3$ for counter-rotating circular geodesics. The critical values q_1, q_2 and q_3 of the quadrupole parameter can be (numerically) determined from Eq. (8.4.11). The difference from the Kerr case is clear instead from Fig. (b): the behaviour of the velocities differs significantly at small distances from the source, whereas it is quite similar for large distances.

A similar discussion concerning the linear velocity $v_{(\mathrm{gmp})}$ of "geodesic meeting point observers" as well as $v_{(\mathrm{ext})}$ of "extremely accelerated observers" is done in Figs. 8.9 and 8.10 respectively.

The behaviours of both the acceleration κ and the first torsion τ_1 as functions of v are shown in Figs. 8.11 and 8.12 for different values of the quadrupole parameter and fixed x as well as for different values of the "radial" distance and fixed q. A number of interesting effects do occur. For instance, from Fig. 8.11 (a) and (b) one recognizes certain counter-intuitive behaviours of the acceleration, in comparison with our Newtonian experience. These effects have their roots also in the Kerr solution and are well known and studied since the 90's. For instance, for negative values of q ($q = -500, -250$) we see that by increasing the speed v (for positive values over that corresponding to the local minimum) the acceleration also increases; hence, in order to maintain the orbit, the particle (a rocket, say) should accelerate outwards. This is counter-intuitive in the sense that for a circular orbit at a fixed radius increasing the speed corresponds to an increase of the centrifugal acceleration and therefore to maintain the orbit "classically" one would expect to supply an acceleration inward. All such effects have been analyzed in the past decades in the Kerr spacetime in function of the radius of the orbit, i.e. the distance from the black hole. The novelty here is represented by Fig. 8.11 (a) where the various curves do not correspond to different orbital radii (i.e. different values of the coordinate x, as it is for the cases (b) and (c)), but to different values of the quadrupole parameter q at a fixed radial distance. Therefore, the conclusion is that a spacecraft orbiting around an extended body –according to general relativity and the QM solution– should expect counter-intuitive engine acceleration to remain on a given orbit. Outward or inward extra acceleration for an increase of the speed critically depend on the quadrupole moment (i.e. the physical structure) of the source, a fact that should be taken into account.

Fig. 8.12 shows instead that at a fixed radius one can always find a value of the quadrupole parameter and a value of the speed at which the first torsion vanishes. Being the second torsion identically vanishing, in these con-

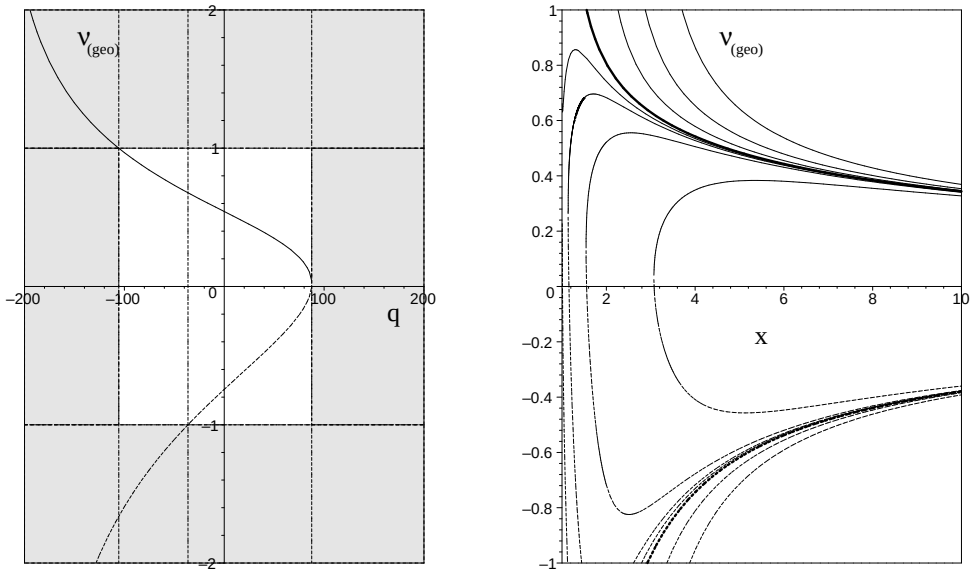

(a) (b)

Figure 8.8: The geodesic linear velocities $\nu^{\pm}_{(\mathrm{geo})}$ are plotted in Fig. (a) as functions of the quadrupole parameter q for fixed distance parameter $x = 4$ from the source and $a/M = 0.5$. Co-rotating and counter-rotating circular geodesics exist for $q_1 < q < q_3$ and $q_2 < q < q_3$ respectively, with $q_1 \approx -105.59$, $q_2 \approx -36.29$ and $q_3 \approx 87.68$ for this choice of parameters. The behaviour of $\nu^{\pm}_{(\mathrm{geo})}$ as functions of x is shown in Fig. (b) for different values of $q = [-80, -30, -10, 0, 2, 4, 10, 50]$. The thick curves correspond to the Kerr case ($q = 0$). Curves corresponding to great positive value of the quadrupole parameter in the allowed range exhibit both a local maximum ($\nu^{+}_{(\mathrm{geo})}$) and a local mimimum ($\nu^{-}_{(\mathrm{geo})}$). For decreasing values of q the local minimum first disappears; for q further decreasing also the local maximum disappears (the curves are thus ordered from left to right for increasing values of q). Curves corresponding to negative values of q never present extrema as in the case of Kerr spacetime ($q = 0$), the lightlike condition being reached at greater values of the "radial" distance for decreasing values of q.

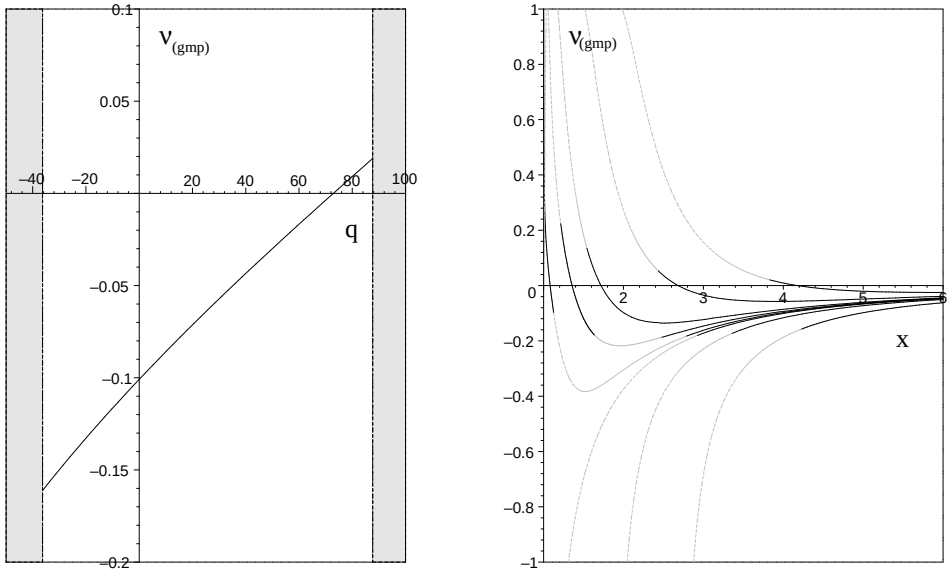

(a) (b)

Figure 8.9: The linear velocity $\nu_{(\mathrm{gmp})}$ corresponding to the "geodesic meeting point observers" is plotted in Fig. (a) as a function of the quadrupole parameter q for fixed distance parameter $x = 4$ from the source and $a/M = 0.5$. The behaviour of $\nu_{(\mathrm{gmp})}$ as a function of x is shown in Fig. (b) for different values of $q = [-50, -10, 0, 2, 5, 10, 30, 80]$. It exists only in those ranges of x where both $\nu^{+}_{(\mathrm{geo})}$ and $\nu^{-}_{(\mathrm{geo})}$ exist (solid black lines). These ranges are listed below: $q = -50$, $x \gtrsim 4.23$; $q = -10$, $x \gtrsim 3.36$; $q = 0$, $x \gtrsim 2.92$; $q = 2$, $1.0012 \lesssim x \lesssim 1.13$ and $x \gtrsim 2.79$; $q = 5$, $1.21 \lesssim x \lesssim 1.64$ and $x \gtrsim 2.48$; $q = 10$, $x \gtrsim 1.54$; $q = 30$, $x \gtrsim 2.44$; $q = 80$, $x \gtrsim 3.83$.

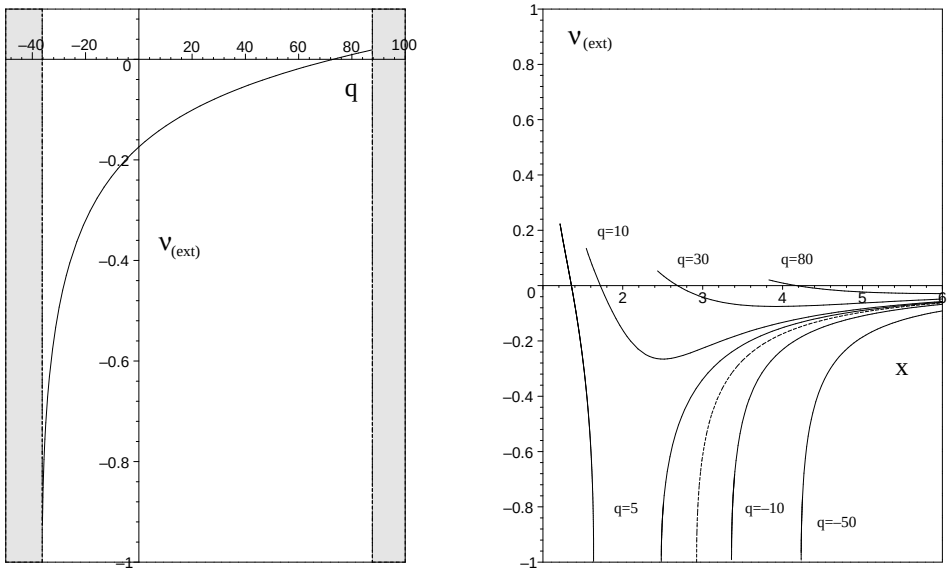

(a) (b)

Figure 8.10: The linear velocity $\nu_{(\mathrm{ext})}$ corresponding to the "extremely accelerated observers" is plotted in Fig. (a) as a function of the quadrupole parameter q for fixed distance parameter $x = 4$ from the source and $a/M = 0.5$. The behaviour of $\nu_{(\mathrm{ext})}$ as a function of x is shown in Fig. (b) for different values of $q = [-50, -10, 0, 5, 10, 30, 80]$. The dashed curve corresponds to the case $q = 0$. It exists only in those ranges of x where both $\nu^{+}_{(\mathrm{geo})}$ and $\nu^{-}_{(\mathrm{geo})}$ exist (see Fig. 8.9).

ditions the Frenet-Serret frame becomes also a Fermi-Walker frame: in fact the Frenet-Serret angular velocity represent the rate of rotation of the Frenet-Serret frame with respect to a Fermi-Walker one. The precession of a test gyroscope (Fermi-Walker dragged along a circular orbit) has been related to the first torsion of an observer-adapted Frenet-Serret frame. The same discussion repeated here together with a simple inspection of Fig. 8.12 allows us to include the effects of the presence of the quadrupole parameter q.

8.5 General form of QM solution with arbitrary Zipoy-Voorhees parameter

The general form of QM solution with arbitrary Zipoy-Voorhees parameter δ is given by Eq. (8.0.1) with functions

$$\begin{aligned} f &= \frac{R}{L} e^{-2q\delta P_2 Q_2} , \\ \omega &= -2a - 2\sigma \frac{\mathfrak{M}}{R} e^{2q\delta P_2 Q_2} , \\ e^{2\gamma} &= \frac{1}{4}\left(1+\frac{M}{\sigma}\right)^2 \frac{R}{(x^2-1)^\delta} e^{2\delta^2 \hat{\gamma}} , \end{aligned} \tag{8.5.1}$$

where $\hat{\gamma}$ is the same as in Eq. (8.0.3), while

$$\begin{aligned} R &= a_+ a_- + b_+ b_- , \qquad L = a_+^2 + b_+^2 , \\ \mathfrak{M} &= (x+1)^{\delta-1}[x(1-y^2)(\lambda+\mu)a_+ + y(x^2-1)(1-\lambda\mu)b_+] . \end{aligned} \tag{8.5.2}$$

The functions $a_\pm$ and $b_\pm$ are now given by

$$\begin{aligned} a_\pm &= (x\pm 1)^{\delta-1}[x(1-\lambda\mu) \pm (1+\lambda\mu)] , \\ b_\pm &= (x\pm 1)^{\delta-1}[x(\lambda+\mu) \mp (\lambda-\mu)] , \end{aligned} \tag{8.5.3}$$

with

$$\begin{aligned} \lambda &= \alpha(x^2-1)^{1-\delta}(x+y)^{2\delta-2} e^{2q\delta\delta_+} , \\ \mu &= \alpha(x^2-1)^{1-\delta}(x-y)^{2\delta-2} e^{2q\delta\delta_-} . \end{aligned} \tag{8.5.4}$$

The functions $\delta_\pm$ and the constants α and σ are instead the same as in Eqs. (8.0.4) and (8.0.5) respectively.

This solution reduces to the solution (8.0.1)–(8.0.5) for $\delta = 1$.

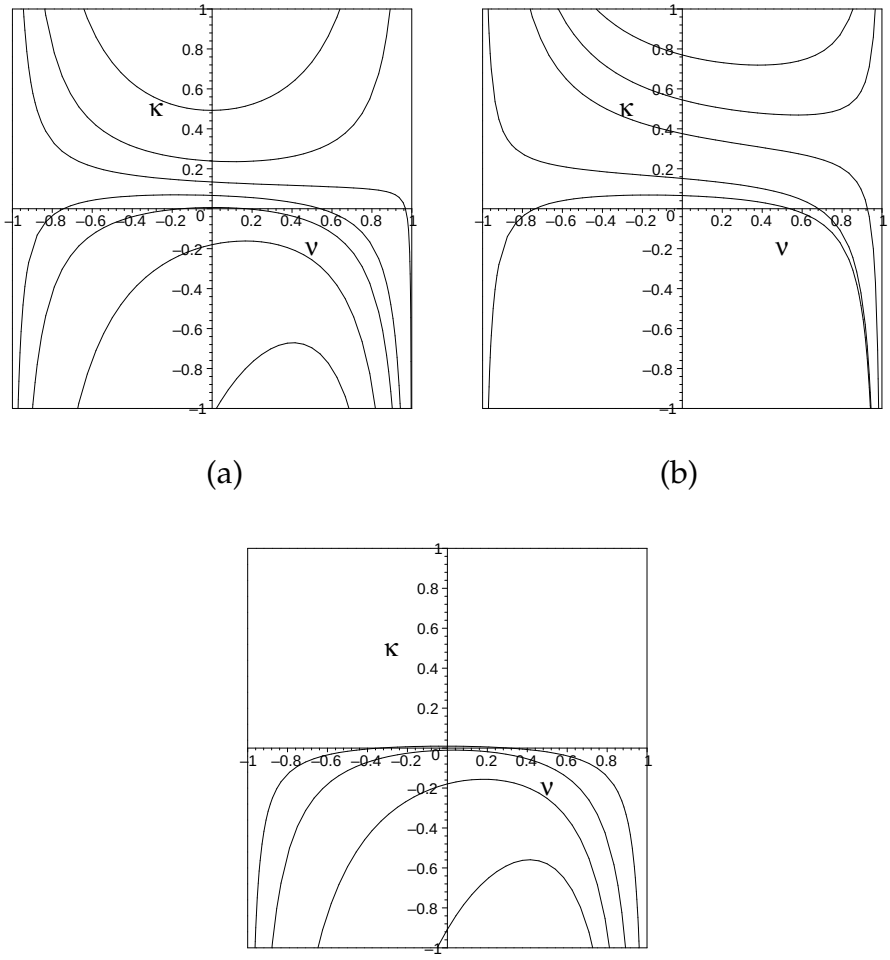

Figure 8.11: The acceleration κ for circular orbits at $y = 0$ is plotted in Fig. (a) as a function of ν for $a/M = 0.5$, $x = 4$ and different values of the quadrupole parameter: $q = [-500, -250, -100, 0, 80, 250, 500]$. The curves are ordered from top to bottom for increasing values of q. The values of ν associated with $\kappa = 0$ correspond to geodesics, i.e. $\nu^{\pm}_{(\mathrm{geo})}$. The behaviour of κ as a function of ν for different x is shown in Figs. (b) and (c) for fixed values of the quadrupole parameter: (b) $q = 1$, $x = [1.1, 1.25, 1.5, 2.5, 4]$ and (c) $q = 100$, $x = [2.5, 3, 4, 10]$.

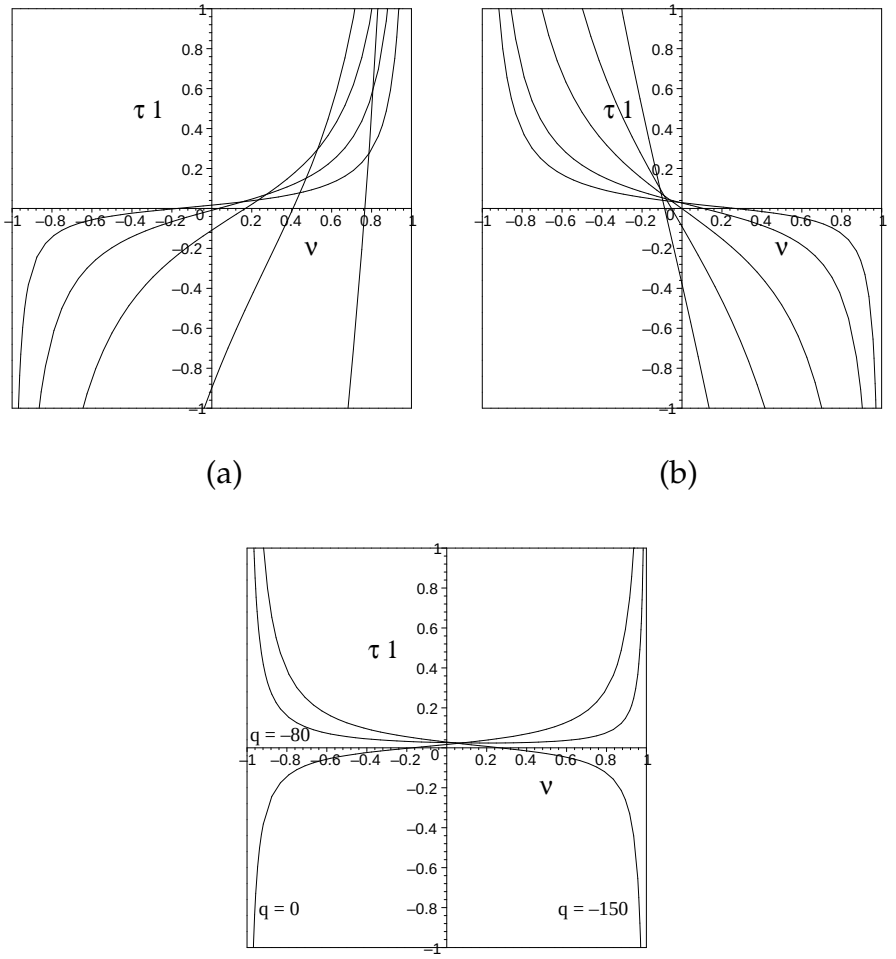

Figure 8.12: The first torsion τ_1 for circular orbits at $y = 0$ is plotted as a function of ν for $a/M = 0.5$, $x = 4$ and different values of the quadrupole parameter: (a) $q = [0, 100, 250, 500, 750]$, (b) $q = [-1000, -750, -500, -250, -150]$ and (c) $q = [-150, -80, 0]$. The curves are ordered from left to right for increasing/decreasing values of q in Fig. (a)/Fig. (b) respectively. Figure (c) shows the changes of behavior occurring in the different regions $q < q_1$, $q_1 < q < q_2$ and $q > q_2$ (see Fig. 8.8).

8.6 Newman-Penrose quantities

Let us adopt here the metric signature $(+,-,-,-)$ in order to use the Newman-Penrose formalism in its original form and then easily get the necessary physical quantities. The Weyl-Lewis-Papapetrou metric is thus given by

$$\begin{aligned} \mathrm{d}s^2 &= f(\mathrm{d}t-\omega\mathrm{d}\phi)^2 \\ &\quad -\frac{\sigma^2}{f}\left\{e^{2\gamma}\left(x^2-y^2\right)\left(\frac{\mathrm{d}x^2}{x^2-1}+\frac{\mathrm{d}y^2}{1-y^2}\right)+(x^2-1)(1-y^2)\mathrm{d}\phi^2\right\} \\ &, \end{aligned} \tag{8.6.1}$$

Introduce the following tetrad

$$\begin{aligned} l &= \sqrt{\frac{f}{2}}\left[\mathrm{d}t-\left(\omega+\frac{\sigma XY}{f}\right)\mathrm{d}\phi\right], \\ n &= \sqrt{\frac{f}{2}}\left[\mathrm{d}t-\left(\omega-\frac{\sigma XY}{f}\right)\mathrm{d}\phi\right], \\ m &= \frac{1}{\sqrt{2}}\frac{\sigma}{\sqrt{f}}e^{\gamma}\sqrt{X^2+Y^2}\left[\frac{\mathrm{d}x}{X}+i\frac{\mathrm{d}y}{Y}\right], \end{aligned} \tag{8.6.2}$$

where

$$X=\sqrt{x^2-1}\,,\quad Y=\sqrt{1-y^2}\,. \tag{8.6.3}$$

The nonvanishing spin coefficients are

$$\begin{aligned} \kappa &= -\mathcal{A}\left[-\frac{XY}{f}(Xf_x+iYf_y)+\frac{f}{\sigma}(X\omega_x+iY\omega_y)+xY-iyX\right], \\ \tau &= -\pi^*=\mathcal{A}(xY-iyX)\,, \\ \nu &= -\mathcal{A}\left[\frac{XY}{f}(Xf_x-iYf_y)+\frac{f}{\sigma}(X\omega_x-iY\omega_y)-xY-iyX\right], \\ \alpha &= \mathcal{A}XY\sigma^4\left[-\frac{1}{2f}(Xf_x-iYf_y)+X\gamma_x-iY\gamma_y-\frac{f}{2\sigma}\left(\frac{\omega_x}{Y}-i\frac{\omega_y}{X}\right)\right. \\ &\quad \left.+\frac{xX+iyY}{X^2+Y^2}\right], \\ \beta &= \mathcal{A}XY\sigma^4\left[\frac{1}{2f}(Xf_x+iYf_y)-X\gamma_x-iY\gamma_y-\frac{f}{2\sigma}\left(\frac{\omega_x}{Y}+i\frac{\omega_y}{X}\right)\right. \\ &\quad \left.-\frac{xX-iyY}{X^2+Y^2}\right], \end{aligned} \tag{8.6.4}$$

where

$$\mathcal{A}=\frac{1}{4}\sqrt{2}\frac{e^{-\gamma}}{\sigma XY}\sqrt{\frac{f}{X^2+Y^2}}\,. \tag{8.6.5}$$

The nonvanishing Weyl scalars are

$$\begin{aligned}
\psi_0 &= \mathcal{A}XY\left[\tau(Xf_x+iYf_y)+2f(X\kappa_x+iY\kappa_y)-\frac{f^2}{\sigma XY}(\kappa+\tau)(X\omega_x+iY\omega_y)\right] \\
&\quad +2\kappa\beta+\tau(\kappa-\tau)\,, \\
\psi_2 &= \frac{1}{6}\frac{\mathcal{A}^2X^2Y^2}{f}\left[x\left(f_x+2f\gamma_x-3i\frac{f^2}{\sigma X^2}\omega_y\right)-y\left(f_y+2f\gamma_y+3i\frac{f^2}{\sigma Y^2}\omega_x\right)\right. \\
&\quad +3i\frac{f}{\sigma}(f_x\omega_y-f_y\omega_x)-X^2(f_{xx}-2f\gamma_{xx})-Y^2(f_{yy}-2f\gamma_{yy}) \\
&\quad \left.+\frac{f^3}{\sigma^2}\left(\frac{\omega_x^2}{Y^2}+\frac{\omega_y^2}{X^2}\right)\right]\,, \\
\psi_4 &= \mathcal{A}XY\left[-\pi(Xf_x-iYf_y)-2f(X\nu_x-iY\nu_y)-\frac{f^2}{\sigma XY}(\nu+\pi)(X\omega_x-iY\omega_y)\right] \\
&\quad +2\nu\alpha+\pi(\nu-\pi)\,. \qquad (8.6.6)
\end{aligned}$$

Finally the two scalar invariants of the Weyl tensor whose ratio defines the speciality index have the following expressions in terms of the Newman-Penrose curvature quantities

$$I=\psi_0\psi_4+3\psi_2^2\,,\qquad J=\psi_0\psi_2\psi_4-\psi_2^3\,,\qquad S=27\frac{J^2}{I^3}\,. \qquad (8.6.7)$$

S has the value 1 for algebraically special spacetimes.

8.7 Remarks

We investigated some properties of the QM spacetime which is a generalization of Kerr spacetime, including an arbitrary mass quadrupole moment. Our results show that a deviation from spherical symmetry, corresponding to a non-zero gravitoelectric quadrupole moment, completely changes the structure of spacetime. A similar behaviour has been found in the case of the Erez-Rosen spacetime. A naked singularity appears that affects the ergosphere and introduces regions where closed timelike curves are allowed. Whereas in the Kerr spacetime the ergosphere corresponds to the boundary of a simply-connected region of spacetime, in the present case the ergosphere is distorted by the presence of the quadrupole and can even become transformed into multiply-connected regions. All these changes occur near the naked singularity.

The presence of a naked singularity leads to interesting consequences in the motion of test particles. For instance, repulsive effects can take place in a region very close to the naked singularity. In that region stable circular orbits can exist. The limiting case of static particle is also allowed, due to the

balance of the gravitational attraction and the repulsive force exerted by the naked singularity.

We have studied the family of circular orbits on the symmetry plane of the QM solution, analyzing all their relevant intrinsic properties, namely Frenet-Serret curvature and torsions. We have also selected certain special circular orbits, like the "geodesic meeting points" orbits (i.e. orbits which contain the meeting points of two oppositely rotating circular geodesics) and the "extremely accelerated" orbits (i.e. orbits with respect to which the relative velocities of two oppositely rotating circular geodesics are opposite), whose kinematical characterization was given in the 90's with special attention to Kerr spacetime. Here we have enriched their properties specifying the dependence on the quadrupole parameter.

The question about the stability of the QM solution is important for astrophysical purposes. In this context, we have obtained some preliminary results by using the variational formulation of the perturbation problem as developed explicitly by Chandrasekhar for stationary axisymmetric solutions. A numerical analysis performed for fixed values of the parameters entering the QM metric shows that it is unstable against perturbations that preserve axial symmetry. One can indeed expect that, once an instability sets in, the final state of gravitational collapse will be described by the Kerr spacetime, the multipole moments of the initial configuration decaying during the black hole formation. Nevertheless, a more detailed analysis is needed in order to completely establish the stability properties of this solution.

Finally, we mention the fact that it is possible to generalize the metric investigated in this work to include the case of a non spherically symmetric mass distribution endowed with an electromagnetic field. The resulting exact solution of Einstein-Maxwell equations turns out to be asymptotically flat, contains the Kerr-Newman black hole spacetime as a special case, and is characterized by two infinite sets of gravitational and electromagnetic multipole moments. For a particular choice of the parameters, the solution is characterized by the presence of a naked singularity. It would be interesting to explore repulsive effects generated by the electromagnetic field of the naked singularity also in this case.

9 Exact and approximate solutions for astrophysical compact objects

In astrophysics, the term compact object is used to refer to objects which are small for their mass. In a wider sense, the class of compact objects is often defined to contain collectively planet-like objects, white dwarfs, neutron stars, other exotic dense stars, and black holes. It is well known that Newtonian theory of gravitation provides an adequate description of the gravitational field of conventional astrophysical objects. However, the discovery of exotic compact objects such as quasars and pulsars together with the possibility of continued gravitational collapse to a black hole points to the importance of relativistic gravitation in astrophysics. Moreover, advances in space exploration and the development of modern measuring techniques have made it necessary to take relativistic effects into account even in the Solar system. It is therefore of importance and interest to describe the relativistic gravitational fields of astrophysical compact objects in terms of their multipole moments, in close analogy with the Newtonian theory, taking into account their rotation and their internal structure.

In this context, the first exterior solution with only a monopole moment was discovered by Schwarzschild (17), soon after the formulation of Einstein's theory of gravity. In 1917, Weyl (4) showed that the problem of finding static axisymmetric vacuum solutions can generically be reduced to a single linear differential equation whose general solution can be represented as an infinite series. The explicit form of this solution resembles the corresponding solution in Newtonian's gravity, indicating the possibility of describing the gravitational field by means of multipole moments. In 1918, Lense and Thirring (18) discovered an approximate exterior solution which, apart from the mass monopole, contains an additional parameter that can be interpreted as representing the angular momentum of the massive body. From this solution it became clear that, in Einstein's relativistic theory, rotation generates a gravitational field that leads to the dragging of inertial frames (Lense-Thirring effect). This is the so–called gravitomagnetic field which is of especial importance in the case of rapidly rotating compact objects. The case of a static axisymmetric solution with monopole and quadrupole moment was analyzed in 1959 by Erez and Rosen (9) by using spheroidal coordinates which are specially adapted to describe the gravitational field of non-spherically symmetric bodies. The exact exterior solution which considers arbitrary values for the angular momentum was found by Kerr only in 1963.

The problem of finding exact solutions changed dramatically after Ernst (2) discovered in 1968 a new representation of the field equations for stationary axisymmetric vacuum solutions. In fact, this new representation was the starting point to investigate the Lie symmetries of the field equations. Today, it is known that for this special case the field equations are completely integrable and solutions can be obtained by using the modern solution generating techniques (12). In this work, we will analyze a particular class of solutions, derived by Quevedo and Mashhoon (20) in 1991, which in the most general case contains infinite sets of gravitational and electromagnetic multipole moments. Hereafter this solution will be denoted as the QM solution.

As for the interior gravitational field of compact objects, the situation is more complicated. There exists in the literature a reasonable number of interior spherically symmetric solutions which can be matched with the exterior Schwarzschild metric. Nevertheless, a major problem of classical general relativity consists in finding a physically reasonable interior solution for the exterior Kerr metric. Although it is possible to match numerically the Kerr solution with the interior field of an infinitely tiny rotating disk of dust, such a hypothetical system does not seem to be of relevance to describe astrophysical compact objects. It is now widely believed that the Kerr solution is not appropriate to describe the exterior field of rapidly rotating compact objects. Indeed, the Kerr metric takes into account the total mass and the angular momentum of the body. However, the moment of inertia is an additional characteristic of any realistic body which should be considered in order to correctly describe the gravitational field. As a consequence, the multipole moments of the field created by a rapidly rotating compact object are different from the multipole moments of the Kerr metric. For this reason a solution with arbitrary sets of multipole moments, such as the QM solution, can be used to describe the exterior field of arbitrarily rotating mass distributions.

In the case of slowly rotating compact objects it is possible to find approximate interior solutions with physically meaningful energy-momentum tensors and state equations. Because of its physical importance, in this work we will study the Hartle-Thorne (22; 23) interior solution which can be coupled to an approximate exterior metric. Hereafter this solution will be denoted as the HT solution. One of the most important characteristics of this family of solutions is that the corresponding equation of state has been constructed using realistic models for the internal structure of relativistic stars. Semi-analytical and numerical generalizations of the HT metrics with more sophisticated equations of state have been proposed by different authors. A comprehensive review of these solutions is given in (21). In all these cases, however, it is assumed that the multipole moments (quadrupole and octupole) are relatively small and that the rotation is slow.

To study the physical properties of solutions of Einstein's equations, Fock (24) proposed an alternative method in which the parameters entering the exterior metric are derived by using physical models for the internal struc-

ture of the body. In this manner, the significance of the exterior parameters become more plausible and the possibility appear of determining certain aspects of the interior structure of the object by using observations performed in the exterior region of the body. Fock's metric in its first-order approximation was recently generalized in 1985 by Abdildin (25) to include the case of a rotating object.

9.1 The Hartle-Thorne metrics

If a compact object is rotating slowly, the calculation of its equilibrium properties reduces drastically because it can be considered as a linear perturbation of an already-known non-rotating configuration. This is the main idea of Hartle's formalism (22). To simplify the computation the following conditions are assumed to be satisfied.
1) There exist an one-parameter equation of state. The matter in equilibrium configuration is assumed to satisfy a one-parameter equation of state, $\mathcal{P} = \mathcal{P}(\mathcal{E})$, where $\mathcal{P}$ is the pressure and $\mathcal{E}$ is the density of total mass-energy.
2) Axial and reflection symmetry. The configuration is symmetric with respect to an arbitrary axis which can be taken as the rotation axis. Furthermore, the rotating object should be invariant with respect to reflections about a plane perpendicular to the axis of rotation
3) Uniform rotation. Only uniformly rotating configurations were considered. It was shown previously that configurations which minimize the total mass-energy (e.g., all stable configurations) must rotate uniformly (26).
4) Slow rotation. It means that angular velocities Ω are small enough so that the fractional changes in pressure, energy density and gravitational field due to the rotation are all less than unity, i.e.

$$\Omega^2 \ll \left(\frac{c}{\mathcal{R}}\right)^2 \frac{GM}{c^2\mathcal{R}} \tag{9.1.1}$$

where M is the mass and $\mathcal{R}$ is the radius of the non-rotating configuration. The above condition is equivalent to the physical requirement $\Omega \ll c/\mathcal{R}$.

Under the above assumptions, the line element for the interior solution is given by

$$ds^2 = \left(1 + \frac{2\Phi}{c^2}\right) c^2 dt^2 - \left[1 + \frac{2R}{c^2}\frac{d\Phi_0(R)}{dR} + \Phi_2(R)P_2(\cos\Theta)\right] dR^2 \\ -R^2\left[1 + \frac{2\Phi_2(R)}{c^2}P_2(\cos\Theta)\right](d\Theta^2 + \sin^2\Theta d\phi^2), \tag{9.1.2}$$

where

$$\Phi = \Phi_0(R) + \Phi_2(R)P_2(\cos\Theta), \tag{9.1.3}$$

is the interior Newtonian potential, Φ_0 is the interior Newtonian potential for the non-rotating configuration, Φ_2 is the perturbation due to the rotation, and $P_2(\cos\Theta)$ is the Legendre polynomial of first kind (22). The interior solution (9.1.2) satisfies Einstein field equations

$$R^{\nu}_{\mu} - \frac{1}{2}\delta^{\nu}_{\mu}R = \frac{8\pi G}{c^4}T^{\nu}_{\mu} \tag{9.1.4}$$

where the stress-energy tensor is that of a perfect fluid

$$T^{\nu}_{\mu} = (\mathcal{E} + \mathcal{P})u^{\nu}u_{\mu} + \mathcal{P}\delta^{\nu}_{\mu}. \tag{9.1.5}$$

The 4-velocity which satisfies the normalization condition $u^{\mu}u_{\mu} = 1$ is

$$u^R = u^{\Theta} = 0, \;\; u^{\phi} = \Omega u^t, \;\; u^t = \left(g_{tt} + 2\Omega g_{t\phi} + \Omega^2 g_{\phi\phi}\right)^{-1/2}, \tag{9.1.6}$$

where the angular velocity Ω is a constant throughout the fluid.

The HT metric describing the exterior field of a slowly rotating slightly deformed object is given by

$$\begin{aligned} ds^2 = \left(1 - \frac{2G\mathcal{M}}{c^2R}\right)\left[1 + 2k_1P_2(\cos\Theta) + 2\left(1 - \frac{2G\mathcal{M}}{c^2R}\right)^{-1}\frac{G^2J^2}{c^6R^4}(2\cos^2\Theta - 1)\right]c^2dt^2 - \\ - \left(1 - \frac{2G\mathcal{M}}{c^2R}\right)^{-1}\left[1 - 2k_2P_2(\cos\Theta) - 2\left(1 - \frac{2G\mathcal{M}}{c^2R}\right)^{-1}\frac{G^2J^2}{c^6R^4}\right]dR^2 \\ - R^2[1 - 2k_3P_2(\cos\Theta)](d\Theta^2 + \sin^2\Theta d\phi^2) + 4\frac{GJ}{c^2R}\sin^2\Theta dt d\phi \end{aligned} \tag{9.1.7}$$

where

$$\begin{aligned} k_1 &= \frac{GJ^2}{c^4\mathcal{M}R^3}\left(1 + \frac{G\mathcal{M}}{c^2R}\right) + \frac{5c^2}{8G^2}\frac{c^2Q - J^2/\mathcal{M}}{\mathcal{M}^3}Q_2^2\left(\frac{c^2R}{G\mathcal{M}} - 1\right), \\ k_2 &= k_1 - \frac{6G^2J^2}{c^6R^4}, \\ k_3 &= k_1 + \frac{G^2J^2}{c^6R^4} - \frac{5}{4G}\frac{c^2Q - J^2/\mathcal{M}}{\mathcal{M}^2R}\left(1 - \frac{2G\mathcal{M}}{c^2R}\right)^{-1/2}Q_2^1\left(\frac{c^2R}{G\mathcal{M}} - 1\right). \end{aligned}$$

Here Q_l^m are the associated Legendre functions of the second kind, and the constants $\mathcal{M}$, J and Q are related to the total mass, angular momentum and mass quadrupole moment of the rotating star, respectively. The HT metric represents an approximate vacuum solution, accurate to second order in the angular momentum J and to first order in the quadrupole parameter Q. In

the case of ordinary stars, such as the Sun, the metric (9.1.8) can be further simplified due to the smallness of the parameters:

$$\frac{G\mathcal{M}_{Sun}}{c^2\mathcal{R}_{Sun}} \approx 10^{-6}, \qquad \frac{GJ_{Sun}}{c^3\mathcal{R}^2_{Sun}} \approx 10^{-12}, \qquad \frac{GQ_{Sun}}{c^2\mathcal{R}^3_{Sun}} \approx 10^{-12}. \tag{9.1.8}$$

There are two ways to incorporate this limit into the metric (9.1.8): either $R \to \infty$ or $c \to \infty$. For the first case, it is necessary that R be a well-defined radial coordinate, whereas the second one can be carried out in an invariant manner only by using the frame theory developed sometime ago by Ehlers (29). The result of the limit $R \to \infty$ has been presented in (23) and the corresponding metric describes the gravitational field of the Sun with an accuracy of one part in 10^{12}. In order to compare in a invariant manner, the HT metric with other metrics we present here the result of applying Ehlers' formalism:

$$ds^2 = \left[1 - \frac{2G\mathcal{M}}{c^2R} + \frac{2GQ}{c^2R^3}P_2(\cos\Theta) + \frac{2G^2\mathcal{M}Q}{c^4R^4}P_2(\cos\Theta)\right]c^2dt^2 + \frac{4GJ}{c^2R}\sin^2\Theta dtd\phi$$
$$- \left[1 + \frac{2G\mathcal{M}}{c^2R} - \frac{2GQ}{c^2R^3}P_2(\cos\Theta)\right]dR^2 - \left[1 - \frac{2GQ}{c^2R^3}P_2(\cos\Theta)\right]R^2(d\Theta^2 + \sin^2\Theta d\phi^2)\,. \tag{9.1.9}$$

The accuracy of this metric is of one part in 10^{18}. Consequently, it describes the gravitational field for a wide range of compact objects, and only in the case of very dense ($G\mathcal{M} \sim c^2\mathcal{R}$) or very rapidly rapidly rotating ($GJ \sim c^3\mathcal{R}^2$) objects large discrepancies will appear.

9.2 Extended first-order approximation metric

Fock's first-order approximation metric was recently derived and investigated by Abdildin (30). Initially this metric was written in its original form in harmonic coordinate system (31; 32) as follows

$$ds^2 = \left[c^2 - 2U + \frac{2U^2}{c^2} - \frac{2G}{c^2}\int\frac{\rho'\left(\frac{3}{2}v^2 + \Pi - U\right)' - P'_{kk}}{|\vec{r} - \vec{r'}|}\left(dx'\right)^3\right]dt^2 -$$
$$- \left[1 + \frac{2U}{c^2}\right]\left(dx_1{}^2 + dx_2{}^2 + dx_3{}^2\right) + \frac{8}{c^2}\left(U_1dx_1 + U_2dx_2 + U_3dx_3\right)dt, \tag{9.2.1}$$

where U is the Newtonian gravitational potential, ρ is the mass density of the body, v is the speed of the particles inside the body (liquid), Π is the elastic energy per unit mass, P_{ik} is the stress tensor, $\vec{U}$ is the gravitational vector potential. Newton's potential satisfies the equation $\Delta U = 4\pi G\rho$. The

solution of this equation which satisfies the asymptotically flatness condition at infinity can be written in the form of a volume integral:

$$U = -G \int \frac{\rho'}{|\vec{r} - \vec{r'}|} dx' dy' dz' \ . \tag{9.2.2}$$

Furthermore, the vector potential must satisfy the equation $\Delta U_i = 4\pi G \rho v_i$ whose general asymptotically flat solution can be represented as

$$U_i = -G \int \frac{(\rho v_i)'}{|\vec{r} - \vec{r'}|} dx' dy' dz'. \tag{9.2.3}$$

In order to completely determine the metric, it is necessary to calculate the above integrals. Clearly, the result will depend on the internal structure of the body which is determined by the density ρ' and velocity v_i' distributions. Once these functions are given, the calculation of the integrals can be performed in accordance with the detailed formalism developed by Fock (24) and then extended and continued by Abdildin (25) and Brumberg (33). Introducing spherical coordinates, the resulting metric can be written as

$$ds^2 = \left[c^2 - \frac{2GM}{r} - \kappa \frac{GS_0^2}{c^2 M r^3} \left(1 - 3\cos^2\theta \right) \right] dt^2 - \left(1 + \frac{2GM}{c^2 r} \right) dr^2 \\ - r^2 \left(d\theta^2 + \sin^2\theta d\phi^2 \right) + \frac{4GS_0}{c^2 r} \sin^2\theta d\phi dt \ , \tag{9.2.4}$$

where S_0 is the angular momentum of the body, M is the total (effective) mass. Here we added the constant κ and verified that in fact the above metric is an approximate solution for any arbitrary real value of κ. This simple observation allows us to interpret Fock's procedure as a method to find out how the internal structure of the object influences the values of the external parameters. For instance, the total mass in the above metric is M but it can decomposed as

$$M = m + \frac{\xi}{c^2}, \tag{9.2.5}$$

where m is the rest mass of the body, and ξ is an arbitrary real constant which, as the constant κ, depends on the internal properties of the body. In particular, the cases of a liquid and a solid sphere have been analyzed in detail with the result

$$\xi = \begin{cases} \frac{8}{3}T + \frac{2}{3}\varepsilon, & \text{for a liquid sphere,} \\ 4T + \frac{2}{3}\varepsilon, & \text{for a solid sphere,} \end{cases} \qquad \kappa = \begin{cases} \frac{4}{7}, & \text{for a liquid sphere,} \\ \frac{15}{28}, & \text{for a solid sphere.} \end{cases} \tag{9.2.6}$$

where T is the rotational kinetic energy of the body and ε is the energy of mutual gravitational attraction of the particles inside the body. In the case

of a static configuration ($S_0 = 0$), the extended metric (9.2.4) reduces to the approximate Schwarzschild metric, where M is the total mass expressed in terms of the internal parameters of the body as given in Eqs.(9.2.5) and (9.2.6). Notice that in this case the field does not depend on the constant κ.

In the general case ($S_0 \neq 0$), the angular momentum of the source generates a gravitational field which, to second order of accuracy in S_0, depends on the constant κ. This opens the possibility of determining the value of κ by measuring the effects of the gravitomagnetic exterior field on test particles. For planet-like compact objects this effect is quite small. Nevertheless, in the case of test particles in the field of more dense sources it should be possible to perform measurements and determine the value of the parameter κ.

9.3 Relation to the Kerr solution

The Kerr metric (19) in Boyer-Lindquist coordinates (35; 33) can be written as

$$ds^2 = \left(1 - \frac{2\mu\varrho}{\varrho^2 + a^2\cos^2\vartheta}\right)c^2dt^2 - \frac{\varrho^2 + a^2\cos^2\vartheta}{\varrho^2 - 2\mu\varrho + a^2}d\varrho^2 - \left(\varrho^2 + a^2\cos^2\vartheta\right)d\vartheta^2 - \\ - \left(\varrho^2 + a^2 + \frac{2\mu\varrho a^2\sin^2\vartheta}{\varrho^2 + a^2\cos^2\vartheta}\right)\sin^2\vartheta d\phi^2 - \frac{4\mu\varrho a\sin^2\vartheta}{\varrho^2 + a^2\cos^2\vartheta}cdtd\phi \tag{9.3.1}$$

where

$$\mu = \frac{GM}{c^2},\ a = -\frac{S_0}{Mc} \tag{9.3.2}$$

Expanding this metric to the order $\frac{1}{c^2}$, one obtains

$$ds^2 = \left[c^2 - \frac{2GM}{\varrho} + \frac{2GMa^2}{\varrho^3}\cos^2\vartheta\right]dt^2 - \left(1 + \frac{2GM}{\varrho c^2} - \frac{a^2}{\varrho^2}\sin^2\vartheta\right)d\varrho^2 - \\ -\varrho^2\left(1 + \frac{a^2}{\varrho^2}\cos^2\vartheta\right)d\vartheta^2 - \varrho^2\left(1 + \frac{a^2}{\varrho^2}\right)\sin^2\vartheta d\phi^2 - \frac{4GMa}{\varrho c}\sin^2\vartheta d\phi dt\ . \tag{9.3.3}$$

Furthermore, if we introduce new coordinates $\varrho = \varrho(r,\theta)$, $\vartheta = \vartheta(r,\theta)$ by means of the equations

$$\varrho = r - \frac{a^2\sin^2\theta}{2r},\ \ \vartheta = \theta - \frac{a^2\sin\theta\cos\theta}{2r^2}\ , \tag{9.3.4}$$

then the Kerr metric (9.3.3) can be reduced to the following form

$$ds^2 = \left[c^2 - 2\frac{GM}{r} - \frac{GS_0^2}{c^2 M r^3}\left(1 - 3\cos^2\theta\right)\right] dt^2 - \left(1 + \frac{2GM}{c^2 r}\right) dr^2 - r^2\left(d\theta^2 + \sin^2\theta d\phi^2\right) + \frac{4GS_0}{c^2 r}\sin^2\theta d\phi dt\,, \quad (9.3.5)$$

which coincides with the metric (9.2.4) with $\kappa = 1$. Consequently, the extended Fock metric (9.2.4) can be interpreted as describing the exterior field of a rotating body to second order in the angular velocity. The advantage of using Fock's method to derive this approximate solution is that it allows to determine the arbitrary constant κ. In fact, whereas $\kappa = \kappa_L = 4/7$ for a liquid sphere and $\kappa = \kappa_S = 15/28$ for a solid sphere, the value for the Kerr metric $\kappa = \kappa_K = 1$ does not seem to correspond to a concrete internal model. On the other hand, all the attempts to find a physically meaningful interior Kerr solution have been unsuccessful. Perhaps the relationship with Fock's formalism we have established here could shed some light into the structure of the interior counterpart of the Kerr metric.

Furthermore, the coordinate transformation (23)

$$r = R - \frac{a^2}{2R}\left[\left(1 + \frac{2G\mathcal{M}}{c^2 R}\right)\left(1 - \frac{G\mathcal{M}}{R}\right) + \cos^2\Theta\left(1 - \frac{2G\mathcal{M}}{c^2 R}\right)\left(1 + \frac{3G\mathcal{M}}{c^2 R}\right)\right], \quad (9.3.6)$$

$$\theta = \Theta - \frac{a^2}{2R^2}\left(1 + \frac{2G\mathcal{M}}{c^2 R}\right)\cos\Theta\sin\Theta\,, \quad (9.3.7)$$

transforms the approximate Kerr solution into the HT solution (9.1.7) with $J = -\mu a$ and a particular quadrupole parameter $Q = J^2/\mu$.

In this way, we have shown that the extended Fock metric coincides for $\kappa = 1$ with the approximate Kerr solution which, in turn, is equivalent to the exterior HT solution with a particular value of the quadrupole parameter. The fact that in the Kerr solution the quadrupole moment is completely specified by the angular momentum is an indication that it can be applied only to describe the gravitational field of a particular class of compact objects. A physically meaningful generalization of the Kerr solution should include a set or arbitrary multipole moments which are not completely determined by the angular momentum. In the next section we present a particular exact solution characterized by an arbitrary quadrupole moment.

9.4 The exact Quevedo-Mashhoon metric

In this section we study the general metric describing the gravitational field of a rotating deformed mass found by Quevedo and Mashhoon (8; 20), which

is a stationary axisymmetric solution of the vacuum Einstein's equations belonging to the class of Weyl-Lewis-Papapetrou (4; 5; 6). For the sake of simplicity we consider here a particular solution involving only four parameters: the mass parameter M, the angular momentum parameter a, the quadrupole parameter q, and the additional Zipoy-Voorhees (36; 37) constant δ. For brevity, in this section we use geometric units with $G = c = 1$. The corresponding line element in spheroidal coordinates (t, r, θ, ϕ) with $r \geq \sigma + M_0,\ 0 \leq \theta \leq \frac{\pi}{2}$ is given by

$$ds^2 = f(dt - \omega d\phi)^2 - \frac{\sigma^2}{f}\left\{e^{2\gamma}\left(d\theta^2 + \frac{dr^2}{M_0^2 - 2M_0 r + r^2 - \sigma^2}\right)\left(\frac{(M_0 - r)^2}{\sigma^2} - \cos^2\theta\right) + \left(\frac{(M_0 - r)^2}{\sigma^2} - 1\right)\sin^2\theta d\phi^2\right\}, \tag{9.4.1}$$

where f, ω and γ are functions of r and θ only, and σ is a constant. They have the form $[x = (r - M_0)/\sigma,\ y = \cos\theta]$

$$f = \frac{R}{L}e^{-2q\delta P_2 Q_2}, \tag{9.4.2}$$

$$\omega = -2a - 2\sigma\frac{\mathfrak{M}}{R}e^{2q\delta P_2 Q_2}, \tag{9.4.3}$$

$$e^{2\gamma} = \frac{1}{4}\left(1 + \frac{M}{\sigma}\right)^2 \frac{R}{(x^2 - 1)^\delta}e^{2\delta^2\hat{\gamma}}, \tag{9.4.4}$$

where

$$R = a_+ a_- + b_+ b_-\ ,\ L = a_+^2 + b_+^2, \tag{9.4.5}$$

$$\mathfrak{M} = (x + 1)^{\delta - 1}\left[x(1 - y^2)(\lambda + \eta)a_+ + y(x^2 - 1)(1 - \lambda\eta)b_+\right], \tag{9.4.6}$$

$$\hat{\gamma} = \frac{1}{2}(1 + q)^2 \ln\frac{x^2 - 1}{x^2 - y^2} + 2q(1 - P_2)Q_1 + q^2(1 - P_2)[(1 + P_2)(Q_1^2 - Q_2^2) + \frac{1}{2}(x^2 - 1)(2Q_2^2 - 3xQ_1Q_2 + 3Q_0Q_2 - Q_2')]. \tag{9.4.7}$$

Furthermore

$$a_\pm = (x \pm 1)^{\delta - 1}[x(1 - \lambda\eta) \pm (1 + \lambda\eta)], \tag{9.4.8}$$

$$b_\pm = (x \pm 1)^{\delta - 1}[y(\lambda + \eta) \mp (\lambda - \eta)], \tag{9.4.9}$$

with

$$\lambda = \alpha(x^2 - 1)^{\delta - 1}(x + y)^{2\delta - 2}e^{2q\delta\delta_+}, \tag{9.4.10}$$

$$\eta = \alpha(x^2-1)^{\delta-1}(x-y)^{2\delta-2}e^{2q\delta\delta_-}, \tag{9.4.11}$$

$$\delta_\pm = \frac{1}{2}\ln\frac{(x\pm y)^2}{x^2-1} + \frac{3}{2}(1-y^2\mp xy) + \frac{3}{4}[x(1-y^2)\mp y(x^2-1)]\ln\frac{x-1}{x+1}, \tag{9.4.12}$$

the quantity α is a constant.

To establish the relationship with the HT solution it is convenient to choose the Zipoy-Voorhees parameter as $\delta = 1+sq$, where s is a real constant. Then, expanding the metric (9.4.1) to first order in the quadrupole parameter q and to second order in the rotation parameter a, we obtain

$$f = 1-\frac{2M}{r}+\frac{2a^2M\cos^2\theta}{r^3}+q(1+s)\left(1-\frac{2M}{r}\right)\ln\left(1-\frac{2M}{r}\right)++3q\left(\frac{r}{2M}-1\right)$$
$$\times\left[\left(1-\frac{M}{r}\right)\left(3\cos^2\theta-1\right)+\left\{\left(\frac{r}{2M}-1\right)(3\cos^2\theta-1)-\frac{M}{r}\sin^2\theta\right\}\ln\left(1-\frac{2M}{r}\right)\right], \tag{9.4.13}$$

$$\omega = \frac{2aMr\sin^2\theta}{r-2M}, \tag{9.4.14}$$

$$\gamma = \frac{1}{2}\ln\frac{r(r-2M)}{(r-M)^2-M^2\cos^2\theta}+\frac{a^2}{2}\left[\frac{M^2\cos^2\theta\sin^2\theta}{r(r-2M)((r-M)^2-M^2\cos^2\theta)}\right]$$
$$+q(1+s)\ln\frac{r(r-2M)}{(r-M)^2-M^2\cos^2\theta}-3q\left[1+\frac{1}{2}\left(\frac{r}{M}-1\right)\ln\left(1-\frac{2M}{r}\right)\right]\sin^2\theta. \tag{9.4.15}$$

The further simplification $s=-1$, and the coordinate transformation (16)

$$r = R+\mathcal{M}q+\frac{3}{2}\mathcal{M}q\sin^2\Theta\left[\frac{R}{\mathcal{M}}-1+\frac{R^2}{2\mathcal{M}^2}\left(1-\frac{2\mathcal{M}}{R}\right)\ln\left(1-\frac{2\mathcal{M}}{R}\right)\right]-$$
$$-\frac{a^2}{2R}\left[\left(1+\frac{2\mathcal{M}}{R}\right)\left(1-\frac{\mathcal{M}}{R}\right)-\cos^2\Theta\left(1-\frac{2\mathcal{M}}{R}\right)\left(1+\frac{3\mathcal{M}}{R}\right)\right] \tag{9.4.16}$$

$$\theta = \Theta-\sin\Theta\cos\Theta\left\{\frac{3}{2}q\left[2+\left(\frac{R}{\mathcal{M}}-1\right)\ln\left(1-\frac{2\mathcal{M}}{R}\right)\right]+\frac{a^2}{2R}\left(1+\frac{2\mathcal{M}}{R}\right)\right\} \tag{9.4.17}$$

transforms the approximate QM solution (9.4.13)–(9.4.15) into the HT solution (9.1.7) with parameters

$$\mathcal{M} = M(1-q),\ \ J=-Ma,\ \ Q=\frac{J^2}{M}-\frac{4}{5}M^3q\,. \tag{9.4.18}$$

Introducing units with $G\neq 1$ and $c\neq 1$, in a similar manner, it is also possi-

ble to show that choosing $\delta = 1 - q$, and expanding the approximate metric (9.4.13)–(9.4.14) in powers of $1/c^2$, the resulting solution can be made to coincide with Fox's extended solution (9.2.4). In other words, the parameter κ turns out to be related with the Zipoy-Voorhees parameter δ.

We presented the main exact and approximate solutions of Einstein's equations which can be used to describe the interior and exterior field of astrophysical compact objects. We found that a particular QM solution, which in general possesses an infinite set of gravitational and electromagnetic multipole moments, contains the exact Kerr metric, as well as the approximate HT and the extended Fock solutions. Moreover, since the HT solution is endowed with its interior counterpart, we conclude that the approximate QM solution (to the second order in the angular momentum and to the first order in the quadrupole parameter) can be matched with the interior HT solution, indicating that it can be used to correctly describe the gravitational field of astrophysical compact objects.

We found that Fock's formalism can be used to construct models for the inner structure of compact objects from which it is possible to determine the parameters of the exterior approximate solution in terms of the inner parameters. A particular parameter which enters the extended Fock metric turns out to have very specific values in the case of a liquid sphere and a solid sphere. In the case of approximate Kerr metric, this parameter does not seem to correspond to any known interior model analyzed in the framework of Fock's formalism. This opens the possibility of attacking the problem of finding the interior counterpart of the exterior Kerr metric by using Fock's method. We expect to investigate this possibility in the near future.

10 Matching with an exact interior solution

Rather few exact stationary solutions that involve a matter distribution in rotation are to be found in the literature. In particular, the interior solution for the rotating Kerr solution is still unknown. In fact, the quest for a realistic exact solution, representing both the interior and exterior gravitational field generated by a self-gravitating axisymmetric distribution of a perfect fluid mass in stationary rotation is considered as a major problem in general relativity. We believe that the inclusion of a quadrupole in the exterior and in the interior solutions adds a new physical degree of freedom that could be used to search for realistic interior solutions. We will study in this section the entire Riemannian manifold corresponding to the simple case of a static exterior solution with only quadrupole moment.

The simplest generalization of the Schwarzschild spacetime which includes a quadrupole parameter can be obtained from the Zipoy–Voorhees solution with $\delta = 1 - q$. The corresponding line element in spherical-like coordinates can be represented as

$$\begin{aligned} ds^2 = & \left(1-\frac{2m}{r}\right)^{1-q} dt^2 \\ & - \left(1-\frac{2m}{r}\right)^{q} \left[\left(1+\frac{m^2\sin^2\theta}{r^2-2mr}\right)^{q(2-q)} \left(\frac{dr^2}{1-\frac{2m}{r}}+r^2 d\theta^2\right) + r^2\sin^2\theta d\varphi^2\right]. \end{aligned} \tag{10.0.1}$$

This solution is axially symmetric and reduces to the spherically symmetric Schwarzschild metric in the limit $q \to 0$. It is asymptotically flat for any finite values of the parameters m and q. Moreover, in the limiting case $m \to 0$ it can be shown that the metric is flat. This means that, independently of the value of q, there exists a coordinate transformation that transforms the resulting metric into the Minkowski solution. From a physical point of view this is an important property because it means that the parameter q is related to a genuine mass distribution, i.e., there is no quadrupole moment without mass. To see this explicitly, we calculate the multipole moments of the solution by using the invariant definition proposed by Geroch (14). The

lowest mass multipole moments M_n, $n = 0, 1, \ldots$ are given by

$$M_0 = (1-q)m\ , \quad M_2 = \frac{m^3}{3} q(1-q)(2-q)\ , \tag{10.0.2}$$

whereas higher moments are proportional to mq and can be completely rewritten in terms of M_0 and M_2. This means that the arbitrary parameters m and q determine the mass and quadrupole which are the only independent multipole moments of the solution. In the limiting case $q = 0$ only the monopole $M_0 = m$ survives, as in the Schwarzschild spacetime. In the limit $m = 0$, with $q \neq 0$, all moments vanish identically, implying that no mass distribution is present and the spacetime must be flat. This is in accordance with the result mentioned above for the metric (10.0.2). Furthermore, notice that all odd multipole moments are zero because the solution possesses an additional reflection symmetry with respect to the equatorial plane.

We conclude that the above metric describes the exterior gravitational field of a static deformed mass. The deformation is described by the quadrupole moment M_2 which is positive for a prolate mass distribution and negative for an oblate one. Notice that in order to avoid the appearance of a negative total mass M_0 the condition $q < 1$ must be satisfied .

10.0.1 Matching conditions

In this subsection we analyze several approaches which could be used to determine the matching hypersurface Σ. Instead of presenting a rigorous analysis, we will present an intuitive method based on the behavior of the curvature and the motion of test particles.

To investigate the structure of possible curvature singularities, we consider the Kretschmann scalar $K = R_{\mu\nu\lambda\tau}R^{\mu\nu\lambda\tau}$. A straightforward computation leads to

$$K = \frac{16m^2(1-q)^2}{r^{4(2-2q+q^2)}} \frac{(r^2 - 2mr + m^2\sin^2\theta)^{2q^2-4q-1}}{(1-2m/r)^{2(q^2-q+1)}} L(r,\theta)\ , \tag{10.0.3}$$

with

$$\begin{aligned} L(r,\theta) = \quad & 3(r-2m+qm)^2(r^2-2mr+m^2\sin^2\theta) \\ & -q(2-q)\sin^2\theta[q^2-2q+3(r-m)(r-2m+qm)] \end{aligned} \tag{10.0.4}$$

In the limiting case $q = 0$, we obtain the Schwarzschild value $K = 48m^2/r^6$ with the only singularity situated at the origin of coordinates $r \to 0$. In general, one can show that the singularity at the origin, $r = 0$, is present for any values of q. Moreover, an additional singularity appears at the radius $r = 2m$ which, according to the metric (10.0.2), is also a horizon in the sense that the

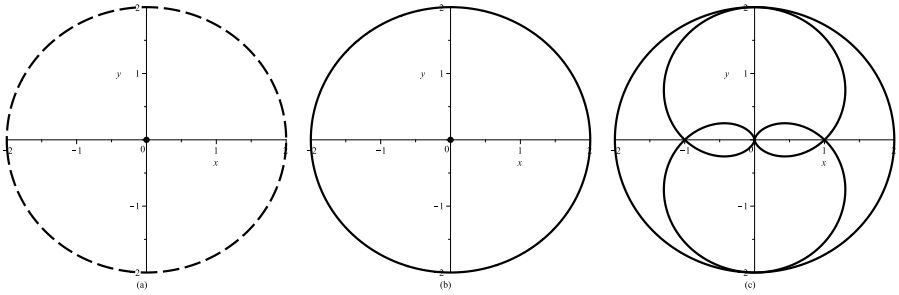

Figure 10.1: Structure of naked singularities of a spacetime with quadrupole parameter q. Plot (a) represents the limiting case of a Schwarzschild spacetime ($q = 0$) with a singularity at the origin of coordinates surrounded by the horizon (dashed curve) situated at $r = 2m$. Once the quadrupole parameter q is included, the horizon transforms into a naked singularity (solid curve) and the central singularity becomes naked as well. This case is illustrated in plot (b). For values of the quadrupole parameter within the interval $q \in \left(1-\sqrt{3/2}, 1+\sqrt{3/2}\right) \setminus \{0\}$, two additional naked singularities appear as depicted in plot (c).

norm of the timelike Killing tensor vanishes at that radius. Outside the hypersurface $r = 2m$ no additional horizon exists, indicating that the singularities situated at the origin and at $r = 2m$ are naked. Moreover, for values of the quadrupole parameter within the interval

$$q \in \left(1-\sqrt{3/2}, 1+\sqrt{3/2}\right) \setminus \{0\} \tag{10.0.5}$$

a singular hypersurface appears at a distance

$$r_{\pm} = m(1 \pm \cos\theta) \tag{10.0.6}$$

from the origin of coordinates. This type of singularity is always contained within the naked singularity situated at the radius $r = 2m$, and is related to a negative total mass M_0 for $q > 1$. Nevertheless, in the interval $q \in (1-\sqrt{3/2}, 1] \setminus \{0\}$ the singularity is generated by a more realistic source with positive mass. This configuration of naked singularities is schematically illustrated in Fig. 10.1.

The analysis of singularities is important to determine the matching hypersurface Σ. Indeed, in the case under consideration it is clear that Σ cannot be situated inside the sphere defined by the radius $r = 2m$. To eliminate all the singularities it is necessary to match the above solution (10.0.2) with an interior solution which covers completely the naked hypersurface $r = 2m$.

Another important aspect related to the presence of naked singularities is the problem of repulsive gravity. In fact, it now seems to be established that naked singularities can appear as the result of a realistic gravitational collapse

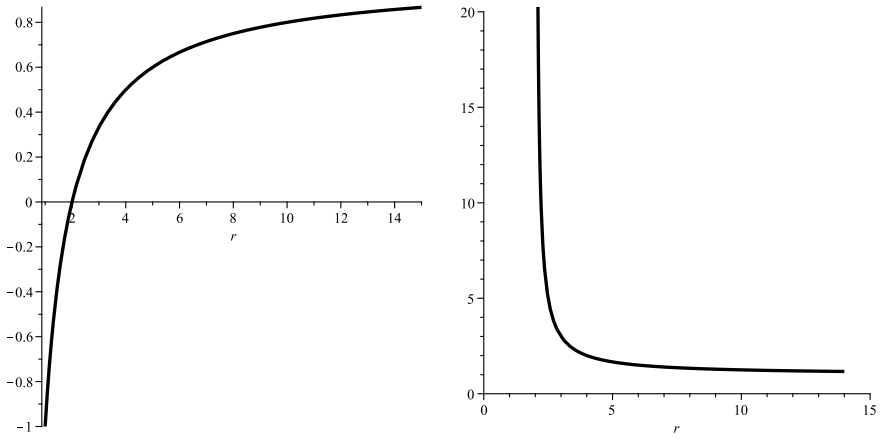

Figure 10.2: The effective potential for the motion of timelike particles. Plot (a) shows the typical behavior of the effective potential of a black hole configuration with $q = 0$. The case of a naked singularity with $q = 1/2$ is depicted in plot (b).

(38) and that naked singularities can generate repulsive gravity. Currently, there is no invariant definition of repulsive gravity in the context of general relativity, although some attempts have been made by using invariant quantities constructed with the curvature of spacetime (39; 40; 41). Nevertheless, it is possible to consider an intuitive approach by using the fact that the motion of test particles in stationary axisymmetric gravitational fields reduces to the motion in an effective potential. This is a consequence of the fact that the geodesic equations possess two first integrals associated with stationarity and axial symmetry. The explicit form of the effective potential depends also on the type of motion under consideration.

In the case of a massive test particle moving along a geodesic contained in the equatorial plane ($\theta = \pi/2$) of the Zipoy–Voorhees spacetime (10.0.2), one can show that the effective potential reduces to

$$V_{eff}^2 = \left(1 - \frac{2m}{r}\right)^{1-q} \left[1 + \frac{L^2}{r^2}\left(1 - \frac{2m}{r}\right)^{-q}\right] , \tag{10.0.7}$$

where L is constant associated to the angular momentum of the test particle as measured by a static observer at rest at infinity. This expression shows that the behavior of the effective potential strongly depends on the value of the quadrupole parameter q. This behavior is illustrated in Fig. 10.2.

Whereas the effective potential of a black corresponds to the typical potential of an attractive field, the effective potential of a naked singularity is characterized by the presence of a barrier which acts on test particles as a source of repulsive gravity. Although this result is very intuitive, the disadvantage of this analysis is that it is not invariant. In fact, a coordinate transforma-

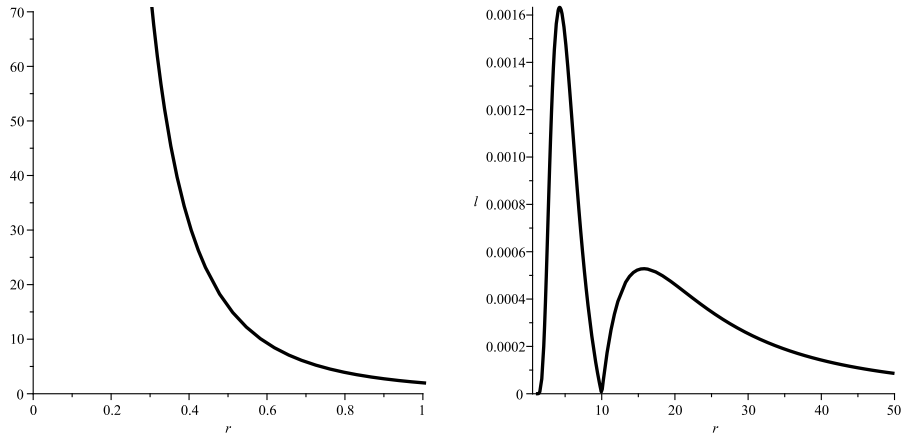

Figure 10.3: Behavior of the curvature eigenvalue on the equatorial plane ($\theta = \pi/2$) of the Zipoy-Voorhees metric. Plot (a) corresponds to a black hole solution with $q = 0$. Plot (b) illustrates the behavior in case of a naked singularity with $q = -2$.

tion can be used to arbitrarily change the position of the barrier of repulsive gravity. Moreover, the identification of the spatial coordinate r as a radial coordinate presents certain problems in the case of metrics with quadrupole moments (42). To avoid this problem we investigate a set of scalars that can be constructed from the curvature tensor and are linear in the parameters that enter the metric, namely, the eigenvalues of the Riemann tensor. Let us recall that the curvature of the Zipoy–Voorhees metric belongs to type I in Petrov's classification. On the other hand, type I metrics possess three different curvature eigenvalues whose real parts are scalars (43). The explicit calculation of the curvature eigenvalues for this metric shows (44) that all of them are real and, consequently, they behave as scalars under arbitrary diffeomorphisms. The resulting analytic expressions are rather cumbersome. For this reason we performed a numerical analysis and found out the main differences between black holes and naked singularities. The results are illustrated in Fig. 10.3.

We took a particular eigenvalue which represents the qualitative behavior of all the eigenvalues. In the case of a black hole, the eigenvalue diverges near the origin of coordinates, where the curvature singularity is situated, and it decreases rapidly as r increases, tending to zero at spatial infinity. In the case of a naked singularity the situation changes drastically. The eigenvalue vanishes at spatial infinity and then increases as the value of the radial coordinate decreases. At a specific radius $r = r_{min}$, the eigenvalue reaches a local maximum and then rapidly decreases until it vanishes. This oscillatory behavior becomes more frequent as the origin of coordinates is approached. It seems plausible to interpret this peculiar behavior as an invariant manifestation of the presence of repulsive gravity. On the other hand, if one would like to avoid the effects of repulsive gravity, one would propose r_{min} as the mini-

mum radius where the matching with an interior solution should be carried out. If we denote the eigenvalue as λ, then r_{min} can be defined invariantly by means of the equation

$$\left.\frac{\partial\lambda}{\partial r}\right|_{r=r_{min}} = 0\,. \tag{10.0.8}$$

Then, the radius r_{min} determines the matching hypersurface Σ and one could interpret condition (10.0.8) as a C^3-matching condition. In concrete cases, one must calculate all possible eigenvalues λ_i and all possible points satisfying the matching condition $\partial\lambda_i/\partial r = 0$. The radius r_{min} corresponds then to the first extremum that can be found when approaching the origin of coordinates from infinity. In the next section we will show that this approach can be successfully carried out in the case of the Zipoy–Voorhees metric.

10.0.2 An interior solution

In the search for an interior solution that could be matched to the exterior solution with quadrupole moment given in Eq.(10.0.2), we found that an appropriate form of the line element can be written as

$$ds^2 = f dt^2 - \frac{e^{2\gamma_0}}{f}\left(\frac{dr^2}{h} + d\theta^2\right) - \frac{\mu^2}{f}d\varphi^2\,, \tag{10.0.9}$$

where

$$e^{2\gamma_0} = (r^2 - 2mr + m^2\cos^2\theta)e^{2\gamma(r,\theta)}\,, \tag{10.0.10}$$

and $f = f(r,\theta)$, $h = h(r)$, and $\mu = \mu(r,\theta)$. This line element preserves axial symmetry and staticity.

The inner structure of the mass distribution with a quadrupole moment can be described by a perfect fluid energy–momentum tensor. In general, in order to solve Einstein's equations completely, pressure and energy must be functions of the coordinates r and θ. However, if we assume that $\rho = \text{const}$, the resulting system of differential equations is still compatible. The assumption of constant density drastically reduces the complexity of the problem. Then, the corresponding field equations reduce to

$$p_r = -\frac{1}{2}(p+\rho)\frac{f_r}{f}\,, \quad p_\theta = -\frac{1}{2}(p+\rho)\frac{f_\theta}{f}\,, \tag{10.0.11}$$

$$\mu_{rr} = -\frac{1}{2h}\left(2\mu_{\theta\theta} + h_r\mu_r - 32\pi p\frac{\mu e^{2\gamma_0}}{f}\right)\,, \tag{10.0.12}$$

$$f_{rr} = \frac{f_r^2}{f} - \left(\frac{h_r}{2h} + \frac{\mu_r}{\mu}\right)f_r + \frac{f_\theta^2}{hf} - \frac{\mu_\theta f_\theta}{\mu h} - \frac{f_{\theta\theta}}{h} + 8\pi\frac{(3p+\rho)e^{2\gamma_0}}{h}\,. \tag{10.0.13}$$

Moreover, the function γ turns out to be determined by a set of two partial

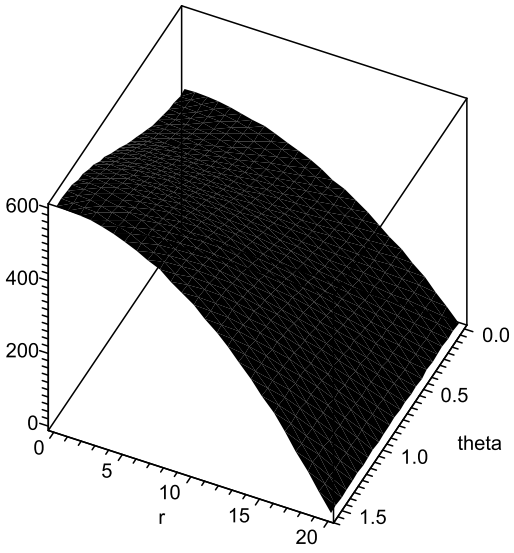

Figure 10.4: Plot of the inner pressure as a function of the spatial coordinates.

differential equations which can be integrated by quadratures once f and μ are known. The integrability condition of these partial differential equations turns out to be satisfied identically by virtue of the remaining field equations.

Although we have imposed several physical conditions which simplify the form of the field equations, we were unable to find analytic solutions. However, it is possible to perform a numerical integration by imposing appropriate initial conditions. In particular, we demand that the metric functions and the pressure are finite at the axis. Then, it is possible to plot all the metric functions and thermodynamic variables. In particular, the pressure behaves as shown in Fig.10.4.

It can be seen that the pressure is finite in the entire interior domain, and tends to zero at certain hypersurface $R(r,\theta)$ which depends on the initial value of the pressure on the axis. Incidentally, it turns out that by increasing the value of the pressure on the axis, the "radius fuction" $R(r,\theta)$ can be reduced. Furthermore, if we demand that the hypersurface $R(r,\theta)$ coincides with the origin of coordinates, the value of the pressure at that point diverges. From a physical point of view, this is exactly the behavior that is expected from a physically meaningful pressure function.

This solution can be used to calculate numerically the corresponding Riemann tensor and its eigenvalues. As a result we obtain that the solution is free of singularities in the entire region contained within the radius function $R(r,\theta)$. In particular, one of the eigenvalues presents on the equatorial plane the behavior depicted in Fig.10.5. All the eigenvalues have a finite value at

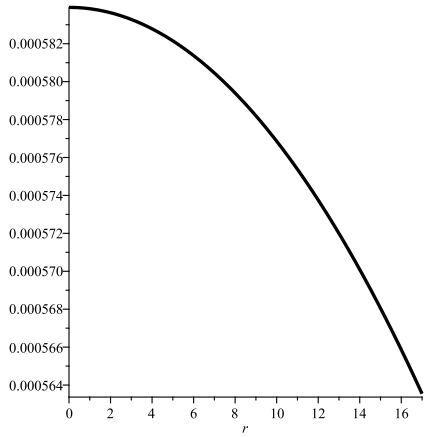

Figure 10.5: Behavior of the curvature eigenvalue on the equatorial plane ($\theta = \pi/2$) of the interior solution.

the symmetry axis and decrease as the boundary surface is approached.

To apply the C^3-matching procedure proposed above we compare the behavior of the eigenvalue plotted in Fig.10.3 with the corresponding eigenvalue plotted in Fig.10.5, using the same scale in both graphics. The result is illustrated in Fig.10.6. It then becomes clear that the first possible point where the matching can be performed is exactly at r_{min} which in this particular case corresponds to $r_{min} \approx 5M_0$. This fixes the initial value of the pressure on the axis which is then used to attack the problem of matching the interior and exterior metric functions. In all the cases we analyzed, we obtained a reasonable matching, withing the accuracy of the numerical calculations. We repeated the same procedure for different values of the angular coordinate ($\theta = \pi/4$ and $\theta = 0$), and obtained that the matching can always be reached by fixing in an appropriate manner the arbitrary constants that enter the metric functions f and μ.

10.1 Concluding remarks

We presented an exact electrovacuum solution of Einstein-Maxwell equations which contains four different sets of multipole moments. An invariant calculation shows that they can be interpreted as the gravitoelectric, gravitomagnetic, electric and magnetic multipole moments. The solution is asymptotically flat and is free of singularities in a region situated around the origin of coordinates. The rotating Kerr metric is contained as a special case. The NUT parameter can also be included by a suitable choice of the arbitrary constants which enter the Ernst potentials. We conclude that this solution can be used to describe the exterior gravitational field a charged rotating mass distribu-

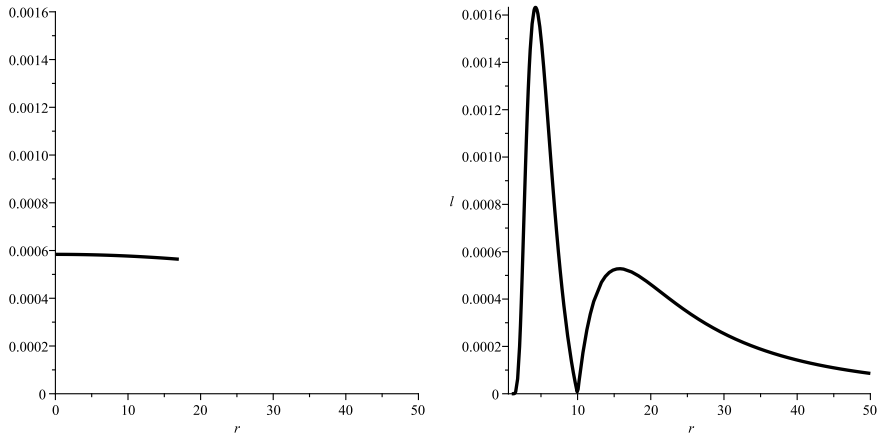

Figure 10.6: Curvature eigenvalues of the interior solution and of the exterior solution with the same scale.

tion.

In the particular case of slowly rotating and slightly deformed mass distribution we obtained the explicit form of the metric, and showed that it can be matched with an interior solution which is contained within the class of Hartle-Thorne solutions. This reinforces the conclusion that the solution represents the interior as well as the exterior gravitational field of astrophysical compact objects.

We studied the problem of matching the interior and exterior spacetimes. We propose a C^3-matching which consists in demanding that the derivatives of a particular curvature eigenvalue are smooth on the matching hypersurface. To prove the validity of this approach we derived an interior solution for the simplest case of a static mass with an arbitrary quadrupole moment, represented by the Zipoy–Voorhees vacuum solution. The numerical integration of the corresponding field equations shows that interior perfect fluid solutions exist which are characterized by a constant density profile with a variable pressure. Fixing the value of the angular coordinate θ, we performed numerically the C^3-matching. As a result we obtain a minimum radius at which the matching can be carried out and a fixed value for the pressure on the symmetry axis. These values are then used to reach the smooth matching of the interior and exterior metric functions. In all the cases analyzed in this manner we obtained a reasonable numerical matching.

The idea of using the C^3-matching condition to determine the minimum radius, at which an interior solution can be matched with an exterior one, has been proved also in a particular case where analytical methods can be applied, namely, in the case of the Kerr-Newman class of solutions. The obtained results are reasonable and compatible with other results obtained by analyzing the motion of test particles (45). These results indicate that

it should be possible to determine the minimum radius of an astrophysical compact object by using the idea of the C^3-matching presented here. To prove this conjecture in general, it will be necessary to use more powerful methods related to the mathematical behavior of geodesics and curvature. This problem is currently under investigation (46). An important application of this analysis would be to relate the minimum size of a compact object with its binding energy. As a result we would obtain the maximum binding energy which is physically allowed for an astrophysical compact object.

For astrophysical applications, the most important multipole moment is the quadrupole one. The importance of the quadrupole has been investigated also very intensively in connection with the motion of extended bodies in general relativity. In particular, the relationship between the interior and the exterior quadrupole moments has been analyzed in detail. The research topic "Symmetries in General Relativity" of this report contains a brief summary of these results.

Bibliography

[1] H. Stephani, D. Kramer, M. MacCallum, C. Hoenselaers, and E. Herlt, Exact solutions of Einstein's field equations, Cambridge University Press, Cambridge UK, 2003.

[2] F. J. Ernst, *New formulation of the axially symmetric gravitational field problem*, *Phys. Rev.* **167** (1968) 1175; F. J. Ernst, *New Formulation of the axially symmetric gravitational field problem II* Phys. Rev. **168** (1968) 1415.

[3] H. Quevedo and B. Mashhoon, *Exterior gravitational field of a rotating deformed mass*, *Phys. Lett. A* **109** (1985) 13; H. Quevedo, *Class of stationary axisymmetric solutions of Einstein's equations in empty space*, *Phys. Rev. D* **33** (1986) 324; H. Quevedo and B. Mashhoon, *Exterior gravitational field of a charged rotating mass with arbitrary quadrupole moment*, *Phys. Lett. A* **148** (1990) 149; H. Quevedo, Multipole Moments in General Relativity - Static and Stationary Solutions-, *Fort. Phys.* **38** (1990) 733; H.Quevedo and B. Mashhoon *Generalization of Kerr spacetime*, *Phys. Rev. D* **43** (1991) 3902.

[4] H. Weyl, *Zur Gravitationstheorie*, *Ann. Physik (Leipzig)* **54** (1917) 117.

[5] T. Lewis, *Some special solutions of the equations of axially symmetric gravitational fields*, *Proc. Roy. Soc. London* **136** (1932) 176.

[6] A. Papapetrou, *Eine rotationssymmetrische Lösung in de Allgemeinen Relativitätstheorie*, *Ann. Physik (Leipzig)* **12** (1953) 309.

[7] F. J. Hernandez, F. Nettel, and H. Quevedo, *Gravitational fields as generalized string models*, Grav. Cosmol. **15**, 109 (2009).

[8] H. Quevedo, *General Static Axisymmetric Solution of Einstein's Vacuum Field Equations in Prolate Spheroidal Coordinates*, Phys. Rev. D **39**, 2904–2911 (1989).

[9] G. Erez and N. Rosen, Bull. Res. Counc. Israel **8**, 47 (1959).

[10] B. K. Harrison, Phys. Rev. Lett. **41**, 1197 (1978).

[11] H. Quevedo, *Generating Solutions of the Einstein–Maxwell Equations with Prescribed Physical Properties*, Phys. Rev. D **45**, 1174–1177 (1992).

[12] W. Dietz and C. Hoenselaers, *Solutions of Einstein's equations: Techniques and results*, (Springer Verlag, Berlin, 1984).

[13] V. A. Belinski and V. E. Zakharov, Soviet Phys. – JETP, **50**, 1 (1979).

[14] R. Geroch, *J. Math. Phys.* **11**, 2580 (1970).

[15] R. O. Hansen, *J. Math. Phys.* **15**, 46 (1974).

[16] D. Bini, A. Geralico, O. Luongo, and H. Quevedo, *Generalized Kerr space-time with an arbitrary quadrupole moment: Geometric properties vs particle motion*, Class. Quantum Grav. **26**, 225006 (2009).

[17] K. Schwarzschild, Sitzungsber. d. Preub. Akad.d.Wissensch., 18 (1916).

[18] H. Thirring and J. Lense, Z. Phys. **19**, 156 (1918).

[19] R. P. Kerr, Phys. Rev. Letters, **11**, 237 (1963).

[20] H. Quevedo and B. Mashhoon, Phys. Rev. D **43**, 3902 (1991).

[21] S. Stergioulas, Living Rev. **7**, (2004).

[22] J. B. Hartle, Astr. J. **150**, 1005 (1967).

[23] J. B. Hartle and K. S. Thorne, Astr. J. **150**, 1005 (1967); 1967 Astr. J. **153**, 807 (1968).

[24] V. A. Fock, *Theory of space, time and gravitation*, (Pergamon Press, London, U.K., 1959)

[25] M. M. Abdildin, *On rotating liquid sphere metric: Questions of field theory* (Alma-Ata University, 1985)

[26] J. Hartle, and D. Sharp, Ap.J., **147**, 317 (1967).

[27] A. Papapetrou, Proc. Roy. Irish Acad. **52**, 11 (1948).

[28] J. B. Hartle and D. H. Sharp, Ap. J., **147**, 317 (1967).

[29] J. Ehlers, *Frame theory* (Springer Verlag, Berlin, 1974)

[30] M. M. Abdildin, *Mechanics of Einstein gravitation theory* (Alma-Ata University, 1988)

[31] De Donder *La gravifique einsteinienne* (Paris, 1921)

[32] K. Lanczos. Phys.ZS. **23**, 537 (1923).

[33] V. A. Brumberg, *Essential Relativistic Celestial Mechanics* (Adam Hilger, Bristol, UK, 1991).

[34] M. M. Abdildin *Bodies motion problem in General Relativity* (Alma-Ata University, 1994)

[35] R. H. Boyer and R. W. Lindquist, J. Math. Phys. **8**, 265 (1967).

[36] D. M. Zipoy, J. Math. Phys. **7**, 1137 (1966).

[37] B. Voorhees, Phys. Rev. D **2**, 2119 (1970).

[38] P. S. Joshi, *Gravitational Collapse and Spacetime Singularities* (Cambridge University Press, Cambridge, 2007).

[39] F. de Felice, *Repulsive gravity and curvature invariants in general relativity*, Ann. de Phys. **14**, 79 (1989).

[40] G. Preti and F. de Felice, *Light cones and repulsive gravity*, Am. J. Phys. **76**, 671 (2008).

[41] C. Cherubini , D. Bini, S. Capozziello, and R. Ruffini, *Second order scalar invariants of the Riemann tensor: Applications to black hole space-times*, Int. J. Mod. Phys. D **11**, 827 (2002).

[42] Ya. V. Zeldovich and I. D. Novikov, *Relativistic Astrophysics* (University of Chicago Press, Chicago, 1971).

[43] P. Jordan, J. Ehlers and W. Kundt, Akad. Wiss. Main. Abh. Math.-Nat. (1960); see also Ref.[1].

[44] H. Quevedo, *Multipole moments in general relativity - Static and stationary solutions* -, Forts. Phys. **38**, 733 (1990).

[45] O. Luongo and H. Quevedo, *Toward an invariant definition of repulsive gravity*, in Proceedings of the 12-th Marcel Grossman Meeting on General Relativity and Gravitation (2010).

[46] R. P. Kerr, H. Quevedo, and R. Ruffini, *On the minimum size of astrophysical compact objects*, in preparation

[47] A. Papapetrou Ann. Inst. H. Poincaré A **4** (1966) 83.

[48] J. Geheniau and R. Debever, Bull. Acad. Roy. Soc. Belgique **42** (1956) 114.

[49] H. Quevedo, Gen. Rel. Grav. **24** (1992) 693.